J. Fluid Mech. (2009), *vol.* 627, *pp.* 97–128.
doi:10.1017/S0022112009005813 Printed in the United Kingdom

Observation of laminar–turbulent transition of a yield stress fluid in Hagen–Poiseuille flow

B. GÜZEL[1], T. BURGHELEA[2], I. A. FRIGAARD[1,3]† AND D. M. MARTINEZ[4]

[1]Department of Mechanical Engineering, University of British Columbia, 2054-6250 Applied Science Lane, Vancouver, BC V6T 1Z4, Canada

[2]Institute of Polymer Materials, University Erlangen-Nurnberg, Martensstrasse 7, D-91058 Erlangen, Germany

[3]Department of Mathematics, University of British Columbia, 1984 Mathematics Road, Vancouver, BC V6T 1Z2, Canada

[4]Department of Chemical and Biological Engineering, University of British Columbia, 2360 East Mall, Vancouver, BC V6T 1Z3, Canada

(Received 3 July 2008 and in revised form 5 January 2009)

We investigate experimentally the transition to turbulence of a yield stress shear-thinning fluid in Hagen–Poiseuille flow. By combining direct high-speed imaging of the flow structures with Laser Doppler Velocimetry (LDV), we provide a systematic description of the different flow regimes from laminar to fully turbulent. Each flow regime is characterized by measurements of the radial velocity, velocity fluctuations and turbulence intensity profiles. In addition we estimate the autocorrelation, the probability distribution and the structure functions in an attempt to further characterize transition. For all cases tested, our results indicate that transition occurs only when the Reynolds stresses of the flow equal or exceed the yield stress of the fluid, i.e. the plug is broken before transition commences. Once in transition and when turbulent, the behaviour of the yield stress fluid is somewhat similar to a (simpler) shear-thinning fluid. Finally, we have observed the shape of slugs during transition and found their leading edges to be highly elongated and located off the central axis of the pipe, for the non-Newtonian fluids examined.

1. Introduction

In this paper, we present results of an experimental study of the laminar, transition and turbulent flows of a visco-plastic fluid in a cylindrical pipe (Hagen–Poiseuille flow). There are the following number of motivations for this study:

(i) Fluids of shear-thinning type with a yield stress abound in industrial settings, as well as some natural ones. Our particular motivation here comes from both the petroleum industry and the pulp and paper industry, where design/control of the inherent processes often requires knowledge of the flow state at different velocities. Similar fluid types and ranges of flows occur in food processing, polymer flows and in the transport of homogeneous mined slurries. Although many of these industrial fluid exhibit more complex behaviour (e.g. thixotropy, visco-elasticity, etc.), as noted by Bird, Armstrong & Hassager (1987), the shear-dependent rheology is often the dominant feature.

† Email address for correspondence: frigaard@mech.ubc.ca

(ii) In line with the above, there is a demand from industrial application to predict the Reynolds number ($Re = UD/\nu$, where U is the average velocity, D is the diameter of the pipe and ν is the kinematic viscosity), or other bulk flow parameter, at which transition occurs, for a range of fluid types, so that different frictional pressure closures may be applied to hydraulics calculations above/below this limit. One of the such earliest attempts, and probably still the most popular, was that of Metzner & Reed (1955). Perhaps the most obvious weakness with such phenomenological formulae is that turbulent transition occurs over a wide range of Reynolds numbers and not at a single number. For example, in careful experiments, Hof, Juel & Mullin (2003) report retaining laminar flows in Newtonian fluids up to $Re = 24\,000$, whereas the common observation of transition initiating in pipe flows is at $Re \approx 2000$. Thus, there is a difficulty with interpreting the predictions of phenomenological formulae, many of which we note were either formulated before a detailed understanding of transitional phenomena has developed. Although such a predictive guideline is a worthy goal, and one we address in a companion paper, it is clear that a necessary precursor to this is a detailed study of transition phenomena, which we provide here.

(iii) A third and most important motivation for our study is scientific. Since Reynolds' famous experiment (Reynolds 1883), transition in pipe flows has been an enduring unsolved problem in Newtonian fluid mechanics. It is thus natural that there have been far fewer studies of non-Newtonian fluids in this regime, either experimental or numerical/theoretical. However, those studies that have been conducted for shear-thinning visco-plastic fluids leave a large number of intriguing questions unanswered. In the first place, experimental studies by Escudier & Presti (1996) using Laponite suspensions and by Peixinho *et al.* (2005) using Carbopol solutions have revealed interesting flow asymmetries in the mean axial velocity profile during transition, which have been largely unexplained. These have been summarized by Escudier *et al.* (2005).

Secondly, although there have been studies of turbulent flows of non-Newtonian fluids there are few detailed studies characterizing the flow phenomena present during transition. Here we focus on the occurrence of puffs and slugs and on an analysis of turbulence statistics. The fluids used in this study are (*a*) Newtonian, (*b*) shear thinning and (*c*) shear thinning with a yield stress $\boldsymbol{\tau}_y$. We compare results between fluid types as the complexity is increased.

Thirdly, yield stress fluids have an axial velocity profile in fully developed laminar flow characterized by an unyielded (or 'plug') zone in the pipe centre. The radius of the plug zone is dictated by a balance between the shear stress and the yield stress of the fluid. With increasing flow rates the size of the plug diminishes but does not vanish, theoretically adopting the role of a rigid solid for the base flow. One of the remaining open questions with these fluids concerns the role of the plug during transition.

Finally, questions arise related to the theoretical side of the problem, where there have been a number of studies of shear instability in flows of visco-plastic fluids, typically for Bingham fluids. Frigaard, Howison & Sobey (1994) studied two-dimensional instabilities of plane channel Poiseuille flow, providing the correct formulation of the stability problem and linearization at the yield surface, but considered odd and even perturbations separately which is questionable for this flow. A recent study by Nouar *et al.* (2007), who implemented the correct conditions at the yield surface, suggests that plane Poiseuille flow is linearly stable at all Re, as is Hagen–Poiseuille flow. Thus, the transitional flow problem is similar in this respect to

that for a Newtonian fluid. Three-dimensional linear instabilities have been studied in Frigaard & Nouar (2003) and transient growth phenomena in Nouar *et al.* (2007). A key feature of the linear stability studies is that the plug region remains unyielded for linear perturbations. This fact can lead to interesting mathematical anomalies. For example, Métivier, Nouar & Brancher (2005) consider the distinguished asymptotic limit of linear stability with small yield stress (vanishing slower than the linear perturbation), which corresponds to a rigid sheet in the centre of a plane channel and is linearly stable. They suggest that the passage to the Newtonian limit of a yield stress fluid is ill defined insofar as questions of stability are concerned. These features reinforce the fundamental interest in plug behaviour during transition, i.e. based on the linear theory the flow is believed to be stable for all Re, but this linear theory itself is based on the continued existence of the plug region.

Apart from the linear analyses, fully nonlinear (energy) stability results are derived in Nouar & Frigaard (2001). As with the Newtonian fluid energy stability results these are very conservative. For yield stress fluids the nonlinearity of the problem is not simply in the inertial terms, but also in the shear stress and in the existence of unyielded plug regions, which are defined in a non-local fashion even for simple flows. This means that the gap between linear and nonlinear theories and between theoretical prediction and experimental evidence is much wider than with Newtonian fluids. Some effort to close this gap has been forthcoming in the form of computational work, e.g. Rudman *et al.* (2004) have conducted direct numerical simulation (DNS) studies with some success, but the need for more experimental study remains and is addressed here.

For Newtonian fluids there is a significant body of experimental work that has focused at flow structure in intermediate transitional regimes. Wygnanski and co-workers (Wygnanski & Champagne 1973; Wygnanski, Sokolov & Friedman 1975) found that flow disturbances evolve into two different turbulent states during transition: puffs and slugs. They observed and described the evolution of localized turbulent puffs and slugs in detail such as their shape, the way they propagate, their velocity profiles and the turbulence intensities inside them. The puff is found when the Reynolds number is below $Re \sim 2700$ and the slug appears when the Reynolds number is above $Re \sim 3000$. Both the puff and slug are characterized by a change in the local velocity in which the flow conditions are essentially laminar outside the structure and turbulent inside. The puff and slug are distinguished from each other by the abruptness of the initial change between the laminar and turbulent states. It has been reported that for a puff, the velocity trace is saw-toothed while a slug has a square form on velocity-time readings. Since these classical studies, many authors have observed and measured puff and slug characteristics in Newtonian fluids. A summary of reported values of the leading U_ℓ and trailing U_t edge velocities of puffs and slugs are given in table 1, scaled by the mean flow velocity U_b.

Further attempts to characterize transition experimentally include the studies of Bandyopadhyay (1986), Toonder & Nieuwstadt (1997), Eliahou, Tumin & Wyagnanski (1998), Han, Tumin & Wyagnanski (2000) and Hof *et al.* (2003). Bandyopadhyay (1986) reports streamwise vortex patterns near the trailing edge of puffs and slugs. Darbyshire and Mullin (1995) indicates that a critical amplitude of the disturbance is required to initiate transition and this value decreases with Re. Toonder & Nieuwstadt (1997) performed Laser Doppler Velocimetry (LDV) profile measurements of a turbulent pipe flow with water. They found that u_{rms} near the wall is independent of Reynolds number. Eliahou *et al.* (1998) investigated experimentally transitional

	U_l/U_b	U_t/U_b	Re	Structure
Wygnanski & Champagne (1973)	0.92	0.86	2200	Puff
Wygnanski & Champagne (1973)	1.55	0.62	8000	Slug
Teitgen (1980)	1.40	0.73	2200	Puff
Draad & J. Westerweel (1996)	1.70	0.60	5800	Slug
Shan *et al.* (1999)	1.56	0.73	2200	Puff
Shan *et al.* (1999)	1.69	0.52	5000	Slug
Mellibovsky & Meseguer (2007)	1.57	0.68	3850	Slug

TABLE 1. Reported literature values of the leading and trailing edge velocities of a puff or a slug in a flowing Newtonian fluid.

pipe flow by introducing periodic perturbations from the wall and concluded that amplitude threshold is sensitive to disturbance's azimuthal structure. Han *et al.* (2000) expanded on the work of Eliahou *et al.* (1998) and advanced the argument that transition is related to the azimuthal distribution of the streamwise velocity disturbances and that transition starts with the appearance of spikes in the temporal traces of the velocity. In addition they found that there is a self-sustaining mechanism responsible for high-amplitude streaks and indicate that spikes not only propagate downstream but also propagate across the flow, approaching the pipe axis. Hof *et al.* (2004) measured the velocity fields instantaneously over a cross-sectional slice of a puff and showed that uniformly distributed streaks exist around the pipe wall and slower streaks exist near the centreline in a puff. They show that the minimum amplitude of a perturbation required to cause transition scales as the inverse of the Reynolds number. There are of course many other experimental studies of Newtonian fluid transition.

The gap between experimental and theoretical understanding of Newtonian shear transition is drawing ever closer. The mid-1990s saw a revival of interest in linear theories with the realization that stable linear modes could undergo prolonged periods of (algebraic) growth before an eventual decay, and that these slowly varying solutions may themselves be unstable. While early work looked for exact resonances, it was later appreciated that due to non-normality of the linearized Navier–Stokes operator, transient growth could occur for specific initial conditions without exact resonance (see Reddy, Schmid & Henningson 1993; Trefethen *et al.* 1993; Chapman 2002 for an overview of these developments). At the same time, self-sustaining mechanisms were proposed by Waleffe and co-workers (Hamilton, Kim & Waleffe 1995; Waleffe 1997), by which energy from the mean flow could be fed back into streamwise vortices, thus resisting viscous decay. Self-sustained exact unstable solutions to the Navier–Stokes equations were found by Faisst & Eckhardt (2003) and by Wedin & Kerswell (2004). Much current effort is focused at understanding the link between these self-sustained unstable solutions and observed transitional phenomena, such as intermittency, streaks, puffs and slugs (see, e.g. Eckhardt *et al.* 2007; Hof *et al.* 2004, 2005; Kerswell & Tutty 2007).

In assessing the literature on non-Newtonian fluid transition, it is important to be specific about the types of fluid that one wishes to study. For example, there is a relatively large literature on drag-reducing polymers (see, e.g. Draad, Kuiken & Nieuwstadt 1998 and the review articles by Berman 1978 and White & Mungal 2008). Frequently, in such studies non-Newtonian features can be interpreted as

a small deviation from the Newtonian behaviour, in particular where the drag reduction is effected via visco-elastic additives. For the fluids we consider, viscometric non-Newtonian effects are a dominant feature of the base laminar flow and we avoid fluids in which visco-elasticity is very significant. Our focus is thus on generalized Newtonian fluids. Simplistically, these are fluids in which the shear stress depends on the strain rate through an effective viscosity η which is a function only of the second invariant ($\dot{\gamma}$) of the strain rate tensor

$$\boldsymbol{\tau}_{ij} = \eta(\dot{\gamma})\dot{\gamma}_{ij}. \tag{1.1}$$

These fluids generally represent those in which shear rheology dominates. Many industrial fluids fall into this class, at least as a first-order description. Well-known rheological models include the Carreau–Yasuda, Cross, Casson, Bingham, power law, Ellis and Herschel–Bulkley models. The two main features of such fluids are shear-thinning behaviour (in which the effective viscosity η decreases with $\dot{\gamma}$), and the possible existence of a yield stress (a threshold in $\boldsymbol{\tau}$ below which $\dot{\gamma} = 0$). Having said this, it is of course impossible to eliminate entirely other rheological effects in using real fluids. Xanthan is known to exhibit elastic effects in addition to its shear-thinning behaviour (and shows drag reducing properties, see e.g. Escudier, Presti & Smith 1999). Carbopol is often used as an experimental fluid for yield shear-thinning behaviour, but at low shear structural thixotropic effects can be quite visible. Other 'model' lab fluids, such as Laponite, are also strongly thixotropic.

There are many studies of these types of fluids in pipe flow. For example, Metzner & Reed (1955) considered a range of experimental data in establishing correlations for frictional pressure losses. Similarly, Hanks & Pratt (1967) present results for yield stress fluids. See also texts such as Govier & Aziz (1972) for an overview of this type of closure model and applications. In the petroleum industry, non-Newtonian pipe flow experiments are commonplace and conducted in order to continually evolve the accuracy of hydraulic predictions (e.g. Shah & Sutton 1990; Willingham & Shah 2000), or in response to new fluid types that are being pumped (e.g. Guo, Sun & Ghalambor 2004). In the mining industry, homogeneous slurries are often modelled as visco-plastic shear-thinning fluids, numerous experimental studies of different flow regimes have been carried out (e.g. Abbas & Crowe 1987; Turian *et al.* 1998), and transitional flow predictions have been developed which are popular within that industry (e.g. Wilson & Thomas 1985, 2006; Slatter 1999; Slatter & Wasp 2000). Many of the approaches we have referenced above are targeted at accurate prediction of frictional pressure losses, with transition simply being considered as the intermediate step between fully laminar and turbulent flows. Thus, these do not study in a direct way the phenomena present in the transitional regime.

In shear-thinning non-Newtonian fluids the change in friction factor is generally much less abrupt on passing through transition (see e.g. various fluids tested in Metzner & Reed 1955; Escudier *et al.* 1999). Thus, although still frequently used, and attractive since easily measurable in hydraulic situations, the accuracy of the friction factor method is certainly diminished. Other common detection methods for Newtonian fluids are based on observations of centreline velocity (as there is a large shift between laminar and turbulent profiles), or the r.m.s. velocity fluctuation

$$u_{rms} = \sqrt{\overline{u'^2}}, \tag{1.2}$$

where $u(t) = \overline{u} + u'(t)$ is the local velocity, or on the turbulence intensity I

$$I = \frac{u_{rms}}{\overline{u}}. \tag{1.3}$$

Park *et al.* (1989) conducted LDA measurements for both laminar and turbulent flows of an oil-based transparent slurry with visco-plastic behaviour. They report that, due to the yield stress, there was very little difference between turbulent and laminar velocity profiles, hence detecting transition via the centreline velocity was ineffective. They advocated use of the turbulent intensity close to the wall, e.g. at 80 % of the radius, which is also adopted by Escudier *et al.* (1999). On the other hand, Peixinho (2004), Peixinho *et al.* (2005) do manage to identify transition from centreline velocity data, although the detection is clearer for the fluids used other than Carbopol.

Flow asymmetries in the mean velocity profiles were first reported by Escudier & Presti (1996), who studied the flow of Laponite solutions in laminar, transitional and fully turbulent flows. They report asymmetry in the range $Re \in [1300, 3000]$. However, under all flow conditions they find that thixotropic effects are observable and the fluid is rarely at its equilibrium shear rheology, except in a very thin wall layer. This clouded any clear interpretation of the asymmetries. Peixinho (2004) conducted pipe and annular flow experiments for CMC and Carbopol solutions. In the transitional regime Peixinho (2004) did not report observing flow asymmetries, although these were apparently evident and are reported later in Peixinho *et al.* (2005). It is worth noting that asymmetric velocity profiles have been observed for Newtonian fluid flows, but under different flow conditions (see Leite 1959).

Peixinho *et al.* (2005) suggest that for yield stress fluids the transition takes place essentially in two stages. In the first stage the turbulence intensity is at laminar levels on the pipe centreline while larger nearer the wall. It is unclear whether or not the plug is broken or intact, but it is suggested that due to the large fluctuations in effective viscosity, flow instabilities generated near the wall could be damped nearer the centre of the pipe. The aspect of flow asymmetry in transition is returned to by Escudier *et al.* (2005). The authors summarize the work of Escudier & Presti (1996), Peixinho *et al.* (2005) and a third independent study, in all of which asymmetry was observed in the mean velocity profiles. The authors discuss the possible effect of the Coriolis force on flow asymmetry (following Draad & Nieuwstadt 1998), concluding that for the more viscous non-Newtonian fluids the Ekman number is simply too large for this to be a viable explanation. Other possible sources of experimental influence are also examined, with the conclusion that the asymmetry has fluid mechanics origins and is not due to imperfections in either the apparatus or measurement technique.

An outline of our paper is as follows: In § 2 we describe the experimental flow loop and the LDV system used to characterize the radial velocity profiles for three different fluid systems. Here we measure velocity profiles across the diameter of the pipe as a function of flow rate. We span the flow rate ranges so that we observe laminar, transitional and turbulent behaviours. In § 3 we present the results in two subsections. In the first subsection, we describe phenomenologically the behaviour of the different fluids undergoing transition. In this subsection we characterize the flow field both using high-speed video images and simple measurements of the fluctuations of the instantaneous velocity measurements. In the next subsection, we characterize the transition to turbulence using higher order statistical methods. In § 4 we summarize the evidence for the breakup of the plug region before transition. In § 5 we highlight the major findings and attempt to give some physical insight into our experimental observations.

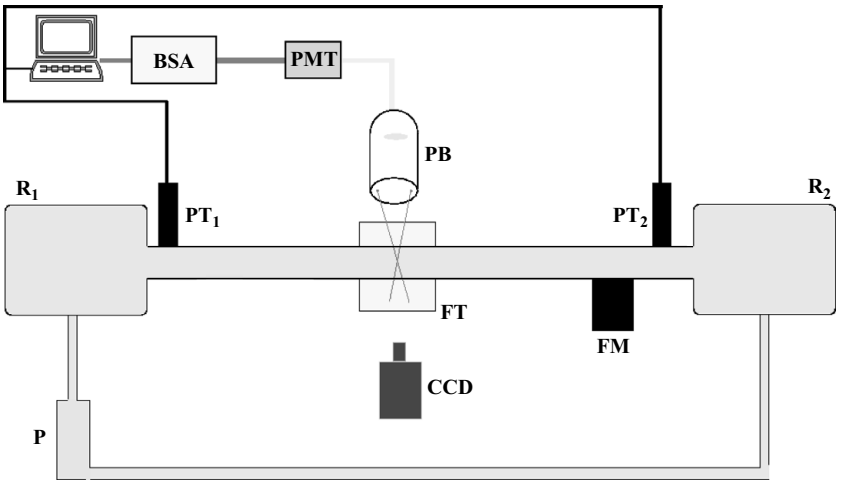

FIGURE 1. Schematic view of the experimental setup: $R_{1,2}$: fluid reservoirs, P: pump, FM: flow meter, $PT_{1,2}$: pressure transducers, FT: fish tank, CCD: digital camera, PB: laser Doppler velocimetry probe, PMT: photomultiplier and BSA: burst spectrum analyzer.

2. Experimental setup and procedures

All results reported are from tests performed in a 10 m long flow loop with an inner diameter of 50.8 mm. The setup is illustrated schematically in figure 1. The flow is generated by a variable-frequency-driven screw pump fed to a carbon steel inlet reservoir R_1 of approximately $120L$ capacity to an outlet reservoir R_2 of the same capacity. The pump can provide a maximum flow rate of $\approx 22\ \mathrm{l\,s^{-1}}$, which is equivalent to a maximal mean flow velocity of $\approx 10\ \mathrm{m\,s^{-1}}$. Two honeycomb sections are placed inside the reservoir R_1 before the tube inlet in order to suppress any swirl or other fluid entry effects. We used a Borda style entry condition in which the pipe extended backwards approximately 50 cm into the tank. Two honeycomb elements were inserted into this section. The fluid reservoir R_2 is pressurized to damp mechanical vibrations induced by the pump motor and a flexible hose is used between the pump and reservoir in order to diminish flow pulsations. The flow channel is constructed of 16 identical sections, 61 cm in length each, joined with flanges and aligned horizontally with the aid of a laser.

The test section of the pipe (placed at about 5.5 m downstream) is fitted with a 'fish tank' FT which consists of a rectangular transparent acrylic box filled with an index-matched fluid (glycerol) in order to minimize the effects of refraction. Velocity measurements are made by using an LDV system from TSI instruments (www.tsi.com). The LDV comprises a 400 mW argon-ion laser (wavelength 457–514 nm), a two-component probe (PB) housing the transmitting and receiving optics, a colour separator and a burst spectrum analyzer (BSA). The probe is mounted on a three-axis translational stage with a spatial resolution of 10 μm. The working fluids are seeded with silver coated hollow glass spheres, 10 μm in diameter, in order to enhance the LDV signal. The LDV optical parameters are as follows:

(*a*) the probe beam diameter is 2.82 mm
(*b*) the beam separation at its front lens is 50 mm
(*c*) the focal length of receiving lens is 362.6 mm
(*d*) the diameter of the measurement volume is 0.0858 mm (measured in air).

Two pressure transducers ($PT_{1,2}$) are located near the inlet and outlet of the flow channel (Model 210, Series C from www.gp50.com). These are bonded strain gauge transducers with internal signal conditioning to provide a Vdc output signal in direct proportion to the input pressure. The accuracy of each transducer is 0.02 % of the full scale and they were calibrated with an externally mounted pressure gauge. Pressure readings were averaged over 150 s and used to estimate the radius of the plug (see (4.1)). Flow rates were estimated using two methods: (i) using an electromagnetic flow metre (FM) installed near the outlet reservoir (see figure 1); (ii) by numerically integrating the measured axial velocity profiles. The latter estimate is used to calculate the relevant flow parameters reported throughout the paper.

Before proceeding it is instructive to estimate if the flow is fully developed at this measurement location. The case to consider is that of a laminar flow of a Newtonian fluid as it is widely known that the entry length for turbulent flows (Nukuradse 1932; Laufer 1952; Perry & Abell 1978; Doherty *et al.* 2007) and for flows with non-Newtonian fluids (Bogue 1959; Chen 1973; Soto & Shah 1976; Froishter & Vinogradov 1980; Bewersdorff 1991) is shorter. For the laminar case, Durst *et al.* (2005) report that it is widely accepted that the entry length L_e/D scales with $Re/30$; there is however a wide variation in this estimate (see Durst *et al.* 2005; Poole & Ridley 2007). With this, at $Re = 3000$ the entry length in our apparatus is roughly $Le/D = 100$. This is significantly shorter than the position of our measurement point, i.e. $Le/D = 108$. In addition to satisfying this criterion, we examined a second criterion to establish if the flow was fully developed. Like Durst *et al.* (2005) and Poole & Ridley (2007), we examined the measured centreline velocity and compared this to an estimated velocity using the pressure drop and viscosity of the fluid. We found that for all cases tested there was less than a 1 % deviation from these results.

The experimental procedure consisted of the following steps:

(*a*) Each fluid tested was mixed *in situ* by circulating the fluids through the flow channel for 5–6 h. The test fluid was then allowed to rest for 4–5 days so that any entrained air bubbles may be dissipated. A fluid sample was then obtained from the reservoir tank and used for subsequent rheological evaluation.

(*b*) During each run, the temperature of the fluid varied by less than 1 °C. No active measures were made to control temperature in this experiment. At the start of an experimental sequence, the desired flow rate was set and the flow loop was then run for a period of time until the temperature stabilized. Once stabilized data acquisition commenced. In this case we record both the volumetric flow rate and instantaneous pressure at a sampling rate of 500 Hz.

(*c*) The velocity profile was measured stepwise across the diameter of the pipe in 1.25 mm increments. At each radial position, the flow was sampled for approximately 150 s at an average rate of 1000 Hz. This data was also used to estimate the local strain rate $\dot{\gamma}$. To do so the derivative was estimated by using a second-order finite difference scheme with a step size of 1.25 mm (2.5 % of the diameter of the pipe), between adjacent nodes. The time-average value at each nodal point was estimated from approximately one-hundred thousand readings; the coefficient of variation was much less than 1 %. Given this large number of data points, the difference between the averages of velocity between adjacent points was statistically significant and the error on this time average derivative is low.

(*d*) At the end of the traverse a fluid sample was obtained, the flow rate increased and the measurement traverse repeated.

Fluid	*Concentration* (wt%)	Velocity U_b (m s^{-1})	Re_G
Glycerin	80	0.37–1.49	731–4442
Glycerin	65	0.06–1.95	342–14180
Xanthan	0.05	0.17	1984
Xanthan	0.1	0.38–2.02	1701–24746
Xanthan	0.2	0.46–2.59	451–5070
Xanthan	0.2	0.28–3.75	352–11272
Carbopol	0.05 (6.7 pH)	0.14–1.49	356–10960
Carbopol	0.08 (7.1 pH)	0.39–2.92	170–5134
Carbopol	0.10 (6.9 pH)	0.31–3.50	42–3309
Carbopol	0.10 (6.6 pH)	0.11–4.59	6–6032
Carbopol	0.15 (6.8 pH)	0.13–4.84	2.7–2953

TABLE 2. A summary of the experimental conditions tested. For each fluid, at least seven different bulk velocities were chosen to cover the range indicated in the table.

All the fluids used in our experiments were transparent, allowing both LDV flow investigation and direct high-speed flow imaging. In total 11 different fluids were tested. The experimental limits such as the mean velocities, concentrations and the corresponding generalized Reynolds numbers (denoted by Re_G), for all the fluids we have tested are summarized in table 2. The values given for each fluid represent the minimum flow rate (fully laminar regime) and the maximum flow rate (fully developed turbulent regime) conditions. The Reynolds number may be defined in a number of ways for non-Newtonian fluids. We have defined a generalized Reynolds number by

$$Re_G = \frac{4\rho}{R}\int_0^R \frac{\bar{u}(r)}{\eta(\dot{\gamma}(r))} r \,\mathrm{d}r, \tag{2.1}$$

where ρ and η are the density and effective viscosity of the fluid. The latter depends on the strain rate of the base flow $\dot{\gamma}(r)$, which is calculated locally from the mean axial velocity. For a Newtonian fluid, $Re_G = Re$, and algebraic relations between Re_G and other commonly used non-Newtonian Reynolds numbers may be easily derived. For laminar flows some simple algebraic manipulations yield the expression

$$Re_G = \frac{4\rho u_c^2}{R|p_x|}. \tag{2.2}$$

We note here that both Xanthan and Carbopol solutions may exhibit elasticity at low shear rates, but for the ranges of flow rates considered in our experiments, it is the shear rheology that dominates. As a result, in this work the Xanthan solutions used are modelled as a power-law fluids:

$$\boldsymbol{\tau} = \kappa\dot{\gamma}^n; \quad \eta = \kappa\dot{\gamma}^{n-1}. \tag{2.3}$$

Although the flow curve for Xanthan can be better fitted by the Carreau–Yasuda model or the Cross model, the power-law model is preferred for its simplicity in calculations.

The yield stress fluid, Carbopol, is characterized as a Herschel–Bulkley fluid

$$\boldsymbol{\tau} = \boldsymbol{\tau}_y + \kappa\dot{\gamma}^n; \quad \eta = \boldsymbol{\tau}_y\dot{\gamma}^{-1} + \kappa\dot{\gamma}^{n-1}: \qquad \boldsymbol{\tau} > \boldsymbol{\tau}_y. \tag{2.4}$$

The parameters $\boldsymbol{\tau}_y$, κ and n are commonly referred to as the fluid yield stress, consistency and shear-thinning (power-law) index, respectively.

U (m s^{-1})	γ (s^{-1})	τ_y (Pa)	κ (Pa·s^n)	n	Re_G
0.11202	0.1–24	2	2.05	0.36	5.5
0.4622	0.1–87	1.5	2.01	0.40	67
1.2076	1–220	1.4	1.59	0.43	378
2.0461	5–414	1.3	1.20	0.48	937
2.3218	5–472	1.2	0.92	0.53	1160
3.1146	5–657	1	0.65	0.60	1735
3.9005	5–1261	0.6	0.35	0.65	2920
4.3967	5–1559	0.4	0.20	0.70	4488

TABLE 3. Flow conditions and Herschel–Bulkley parameters for 0.1 % Carbopol.

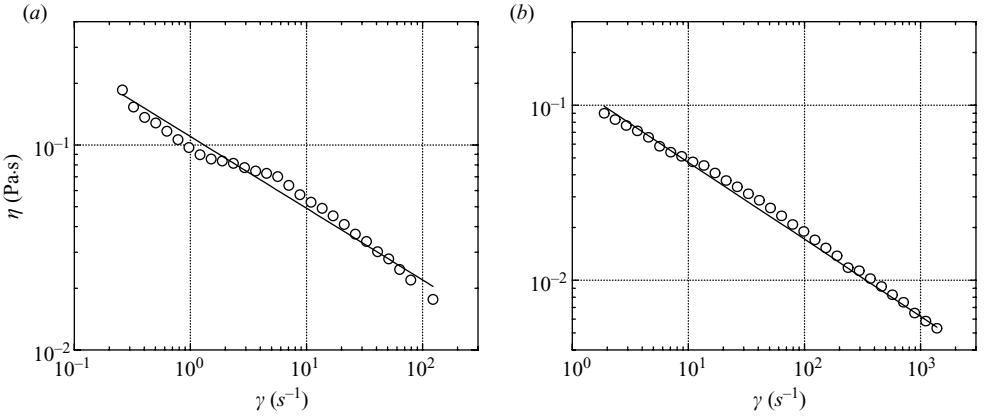

FIGURE 2. Rheograms for 0.2 % Xanthan gum solution, described by the power-law model: (*a*) $\kappa = 0.11$ Pa·s^n, $n = 0.65$; (*b*) $\kappa = 0.13$ Pa·s^n, $n = 0.56$.

The shear rheology of the samples was measured for each fluid sample at the same temperatures as the fluids in the flow loop. Rheological measurements were performed on a controlled-stress rheometer (CVOR 200, from Bohlin, now Malvern Instruments) with a 1° 40 mm cone and plate geometry and 25 mm vane tool. A standard v25 (four blades, vane length 42 mm) vane geometry (www.malvern.co.uk) was employed in these tests and the yield stress was determined by a stress ramp method (Nguyen & Boger 1985). The vane tool was used for measurements of the yield stress because wall slip effects are known to be absent for this geometry. For the viscosity measurements in a high shear rate range (which corresponds to most of our experimental domain) the cone and plate geometry was used. The empirical constants describing the rheological were determined by comparison to both this rheogram and to the laminar velocity profiles measured in the pipe. Degradation is apparent in the rheological properties of the structured fluids. Table 3 details the change in rheology after every flow rate for 0.1 % Carbopol.

Finally, it is widely known that a weakness of both the power law and Herschel–Bulkley models is that there is no high-shear limiting viscosity. Thus, parameter fitting from the flow curve can give different results depending on the range of strain rates used for the fit. Here we fit model parameters from the fluid samples taken before each experiment and use flow curve data that covers the approximate range investigated in the experiment. Figure 2 provides an illustration of how using different strain rate

ranges, for the same fluid, can result in different parametric fits for the same Xanthan solution. Tables of fitted parameters for each experiment reported are given in the Appendix. The parameters fitted obviously have no influence on the results reported here; these are included for completeness and as an aid to future comparisons with computational and theoretical approaches.

Experimental uncertainties caused by small imperfections of the pipe, temperature gradients in the room or degradation of the tested fluids generally have a smaller effect on the calculated Re_G than using incorrect rheological parameters. By 'incorrect', we mean that either the parameter fit is made from data covering the wrong range of strain rates, or the fluid sample is taken from an unyielded/stationary zone in the end reservoirs (as opposed to the yielded parts), or that care is not taken to cross-check the rheological data against the pipe flow velocity profile (in laminar regime only).

The largest errors almost certainly arise in the yield stress. In reality, yielding behaviour is observed over a range of stresses and specifying a single yield stress value is simply a fitting parameter. This range is estimated by using the stress ramp method with vane rheometer measurements. For any given yield stress fitting the other rheological parameters to the flow curve data is a robust procedure. Having determined ranges of rheological parameters we then compare normalized velocity profiles from the LDV measurements with those calculated from the rheological model (which are dimensionlessly parameterized by n and r_p), to determine the final parameters.

Evidently, many different errors contribute to the value of Re_G. A reasonable error estimate for Re_G is obtained by comparing the Re_G that is calculated from the rheological parameters, constitutive law and velocity profile, i.e. (2.1), with that computed from the pressure drop and centreline velocity, i.e. (2.2). For different concentrations of Carbopol, the difference between these two Re_G calculated for the same flows is 1–2 % at smaller Reynolds numbers and increases to 10–15 % at higher Reynolds numbers close to transition. It is interesting to note that at low shear values, where errors in yield stress dominate, the contributions to Re_G in calculating the integrand in (2.1) are smallest, due to the large effective viscosity. The Re_G calculated with pressure drop underestimates the true value of Re_G because the entrance pressure losses are included. For comparison, the difference between these two values of Re_G for glycerin is about 1–5 % for laminar flows.

Note that as velocity profiles become turbulent, due to nonlinearity in the constitutive laws, the effective viscosity of the averaged velocity profile may not be an accurate measure of viscous effects in the flow and a discrepancy between (2.1) and (2.2) is inevitable. More concisely, deriving (2.2) relies on a constitutive law relating the averaged velocity profile (via an effective viscosity) to the mean shear stresses and hence pressure drop. The constitutive relation is not known for the turbulent flow. This same difficulty arises with other commonly used generalized Newtonian fluid Reynolds numbers, which are typically based on the laminar flow characteristics, e.g. the Metzner–Reed Reynolds number.

As with Re_G, we can either evaluate r_p directly from the rheology and velocity profile fit (as we have used in the figures and tables presented below), or we can use the yield stress and measured pressure drop. Since both methods are vulnerable to errors in the yield stress, the level of precision using either estimate is comparable. However, r_p calculated from the pressure drop underestimates the true value because the entry length losses are included in the pressure drop measurement. Values of r_p are about 5–20 % lower than those calculated from the rheology and velocity profile fit.

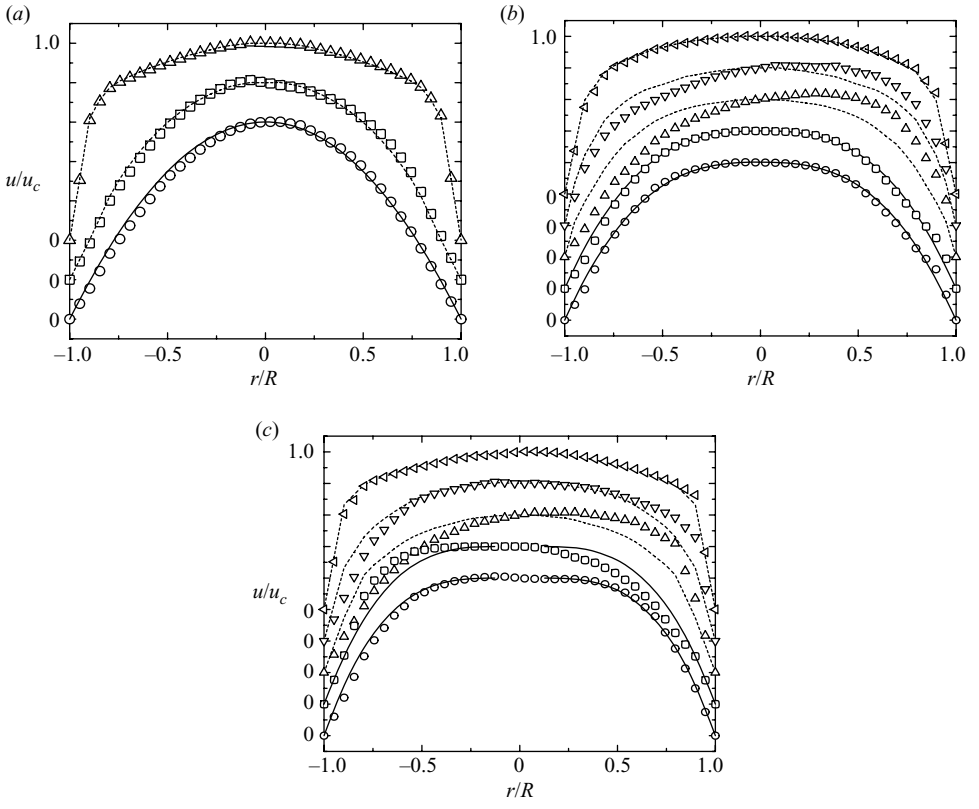

FIGURE 3. The time averaged velocity profiles for the three different fluids tested. (*a*) 65 % glycerin at $Re_G = 633$ (○), 2573 (□) and 10531 (△); (*b*) 0.2 % Xanthan gum at $Re_G = 809$ (○), 1185 (□), 2244 (△), 2542 (▽) and 3513 (◁) and (*c*) 0.15 % Carbopol at $Re_G = 561$ (○), 1120 (□), 1750 (△), 1804 (▽) and 2953 (◁).

3. Results

3.1. *Phenomenological observations*

Before proceeding to the main findings, it is instructive to first examine representative velocity profiles for all fluids and flow states measured. To this end, we plot the time-averaged velocity profiles as a function of Re_G (see figure 3). At each radial position, over one-hundred thousand instantaneous velocity measurements were used in the ensemble average and the confidence interval for each point is very small. It should be noted that the results have been made dimensionless by scaling the ensemble average with the centreline velocity u_c. Under laminar conditions, that is with $Re_G < 1700$, the fully developed laminar profiles are included in these graphs as the solid lines. This was performed in order to ascertain the validity of our results. For the higher flow rates, we present cases for both transitional and turbulent flows. Dashed lines are drawn to highlight an apparent asymmetry in the measurements. The dashed lines were constructed by averaging the data at equivalent radial positions on either side of the central axis. The asymmetry is apparent for the non-Newtonian cases and disappears once full turbulence is achieved. It is worth noting that the asymmetry is systematic, i.e. these data were taken from time-averaged data and the asymmetry is consistently in the same part of the pipe for the same fluid. This is highlighted in figures 4 and 5 where experimental conditions are replicated resulting in a similar bias

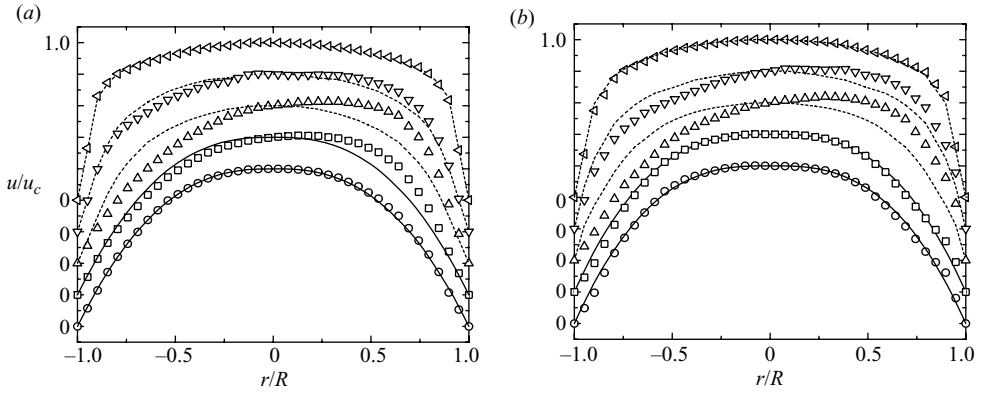

FIGURE 4. The time-averaged velocity profiles for 0.2 % Xanthan gum. These data are from replicate tests obtained from similar experimental conditions (*a*) $Re_G = 858$ (○), 1218 (□), 1900 (△), 2363 (▽) and 3244 (◁); (*b*) $Re_G = 809$ (○), 1185 (□), 2244 (△), 2542 (▽) and 3513 (◁).

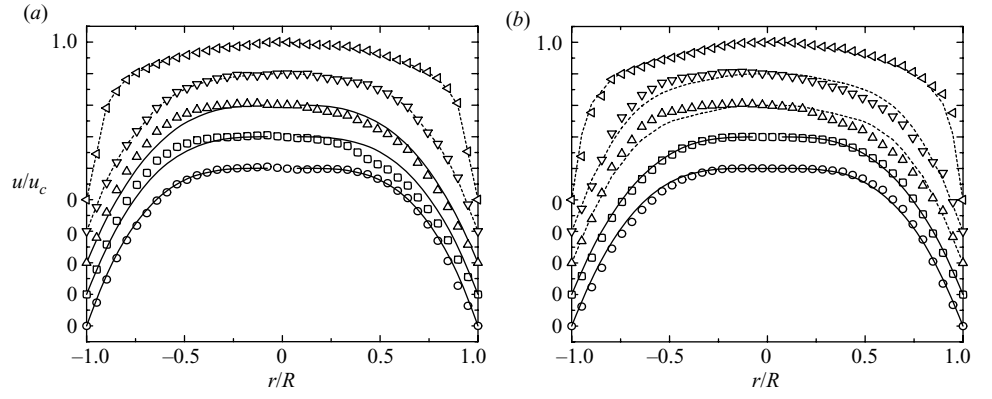

FIGURE 5. The time-averaged velocity profiles for 0.1 % Carbopol. These data are from replicate tests obtained from similar experimental conditions. (*a*) $Re_G = 378$ (○), 937 (□), 1160 (△), 1735 (▽) and 2920 (◁); (*b*) $Re_G = 397$ (○), 914 (□), 2001 (△), 2238 (▽) and 2612 (◁).

in the result. It should be noted in the figures that the asymmetry shows no directional dependence. For different fluids the profiles may be skewed in either direction. This persistence runs contrary to the intuitive notion that transitional flow structures, when ensemble averaged over a suitably long time, should occur with no azimuthal bias. A similar asymmetry has been reported by other groups in their experiments (see e.g. Escudier & Presti 1996; Escudier *et al.* 2005; Peixinho *et al.* 2005). Our initial reaction to the asymmetry was to look for and eliminate any directional bias in the apparatus or in the flow visualization. However, even after extensive precautions the asymmetry still persists. A similar result is observed in the radial profiles of the local r.m.s. of the velocity fluctuation for the non-Newtonian fluids. A representative case is given in figure 6 for a 0.2 % Xanthan gum solution. One can notice from figures 4(*a*) and 6 that the peak asymmetry in u_{rms} profiles is on the opposite side to the asymmetry seen in mean velocity profiles.

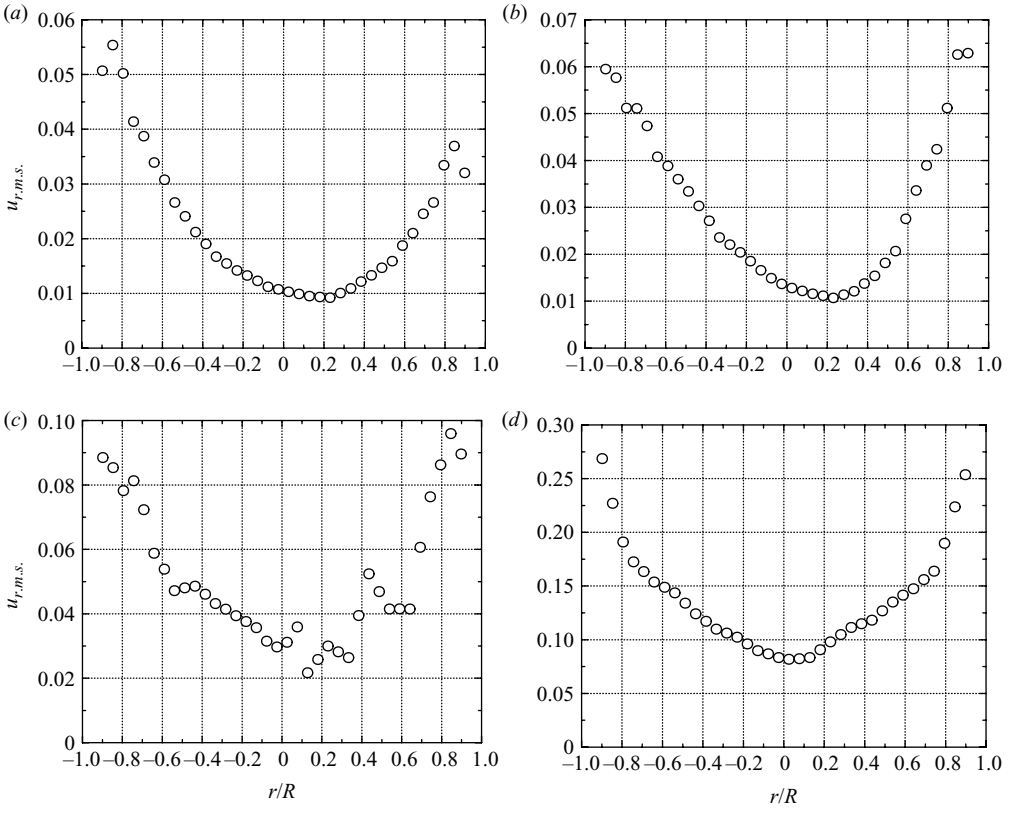

FIGURE 6. Local r.m.s. velocity and mean turbulence intensity profiles for 0.2 % Xanthan Gum; at (*a*) $Re_G = 858$, (*b*) $Re_G = 1218$, (*c*) $Re_G = 1900$ and (*d*) $Re_G = 3244$.

Figure 7 plots the evolution of the turbulent intensity with Re_G, both at the centreline and at radial positions $r/R = \pm 0.75$. Other radial positions could have been displayed, but we chose to show these three as it clearly defines the phenomena that we wish to discuss. To begin, the first observation that can be made is that for Newtonian fluids, (see figure 7*a*), in the laminar regime we see a decay in turbulent intensity as flow rate is increased. This decay is due to having approximately the same magnitude of noise in the system while increasing mean velocity. This is valid for all of the experiments. On transition there is a sharp change in turbulent intensity that occurs across the pipe section simultaneously, i.e. at the same Re_G. After a rapid increase through transition the turbulent intensity relaxes as we enter the fully turbulent regime. For the structured fluids, transition does not involve a simultaneous and sharp increase in turbulent intensity, across the pipe radius. Instead in figures 7(*b*) and 7(*c*) we observe that the turbulent intensity begins to increase at $r/R = \pm 0.75$, at markedly lower Reynolds numbers than at the centreline. A pattern that we noticed that is generally found for the structured fluids tested is that the slope of the curve near transition was rarely negative. This observation will be confirmed below through direct visual observation of turbulent puffs through high-speed imaging. In this study it was difficult to classify the turbulent spot as either a puff or a slug. This is not a unique finding as other research groups without active disturbance control mechanisms report similar findings (Rudman *et al.* 2004). As a result, in the subsequent text we use the term puff and slug synonymously. A simplistic explanation

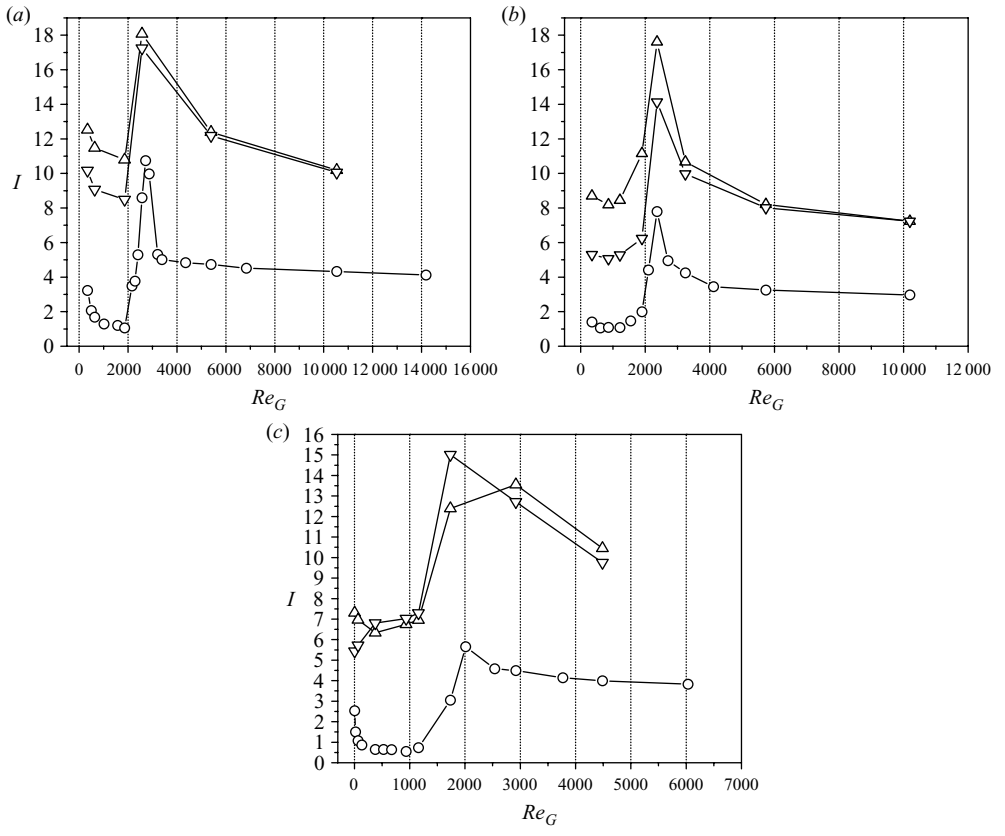

FIGURE 7. Turbulence intensity at $r/R = 0$ (–○–), $r/R = -0.75$ (–△–) and $r/R = 0.75$ (–▽–) for (*a*) 65 % glycerin, (*b*) 0.2 % Xanthan gum and (*c*) 0.1 % Carbopol.

for this different behaviour is that the effective viscosity is usually significantly larger close to the centreline for shear-thinning fluids in laminar flow.

Apart from measuring the axial velocity, we also visualized the flow via seeding particles and a two-coloured art dye, for which the colour changes with the orientation of particles. This enables qualitative evaluation of the flow, i.e. the particles in turbulent structures are of a different colour than the ones in laminar regimes. The images are then processed and some features of the turbulent spots (puff/slug) are derived from these images. The recording station is placed at about 7.6 m downstream. Our imaging system consisted of a Mega Speed MS70K type high-speed video camera (504×504 pixel spatial resolution with a maximum framing rate of 5200 frames s^{-1}) mounted with a 25 mm lens. A typical sequence of images are shown in figure 8 for 0.1 % Xanthan. This is a representative figure which was recorded at 400 frames s^{-1}. The flow in this case proceeds from left to right. In figure 8(*a*)–(k), a turbulent puff is passing the point of observation causing mixing of the tracer particles. This results in a grainy image due to the change in mean orientation, i.e. reflectance, of the tracer particles. In figure 8(*k*), the trailing edge of the puff is observed, and the flow is once again laminar after the puff has passed. A second example from a Carbopol puff is illustrated in figure 9.

With these images we attempted to characterize the size and velocity of the leading and trailing edges of the puff by an object tracking method. We have also produced

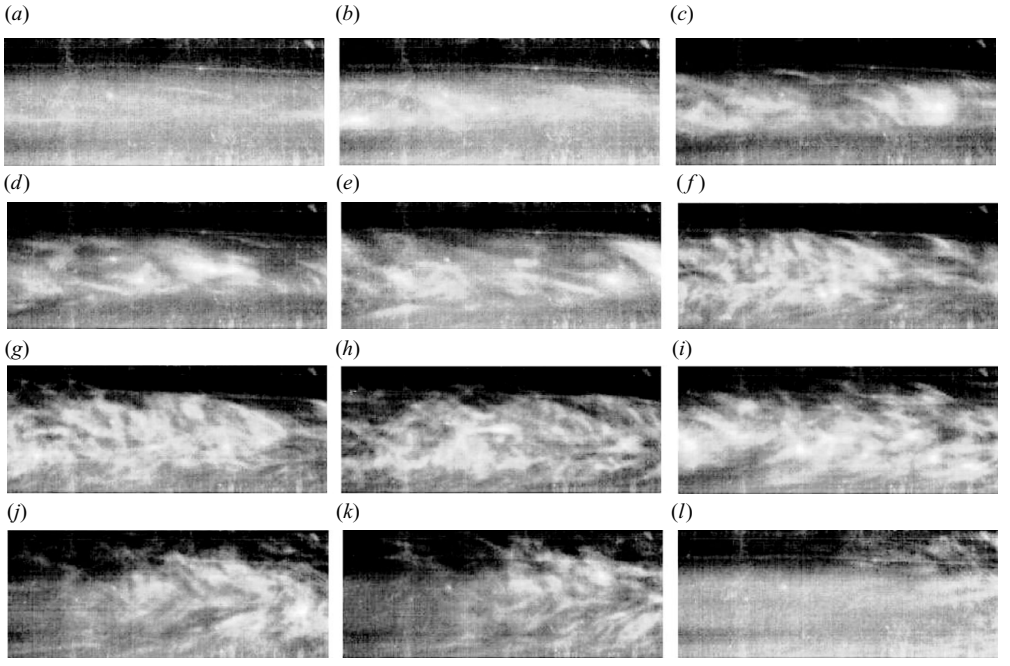

FIGURE 8. Instant puff images taken for 0.1 % Xanthan at $Re_G = 2236$ at different time instants: (*a*) $t = 342.5$ ms, (*b*) $t = 667.5$ ms, (*c*) $t = 842.5$ ms, (*d*) $t = 915$ ms, (*e*) $t = 1005$ ms, (*f*) $t = 1165$ ms, (*g*) $t = 1207.5$ ms, (*h*) $t = 1290$ ms, (*i*) $t = 1675$ ms, (*j*) $t = 4337.5$ ms, (*k*) $t = 4377.5$ ms and (*l*) $t = 4527.5$ ms.

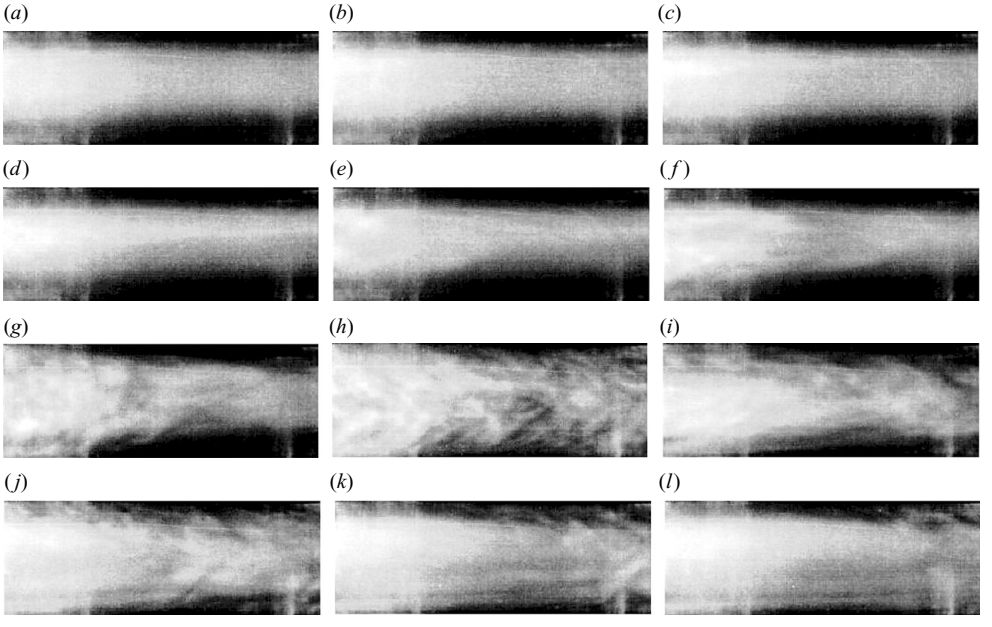

FIGURE 9. Instant puff images taken for 0.075 % Carbopol at $Re_G = 1850$ at different time instants: (*a*) $t = 130$ ms, (*b*) $t = 225.5$ ms, (*c*) $t = 255.5$ ms, (*d*) $t = 320$ ms, (*e*) $t = 422.5$ ms, (*f*) $t = 447.5$ ms, (*g*) $t = 497.5$ ms, (*h*) $t = 600$ ms, (*i*) $t = 755$ ms, (*j*) $t = 1117.5$ ms, (*k*) $t = 1155$ ms and (*l*) $t = 1187.5$ ms.

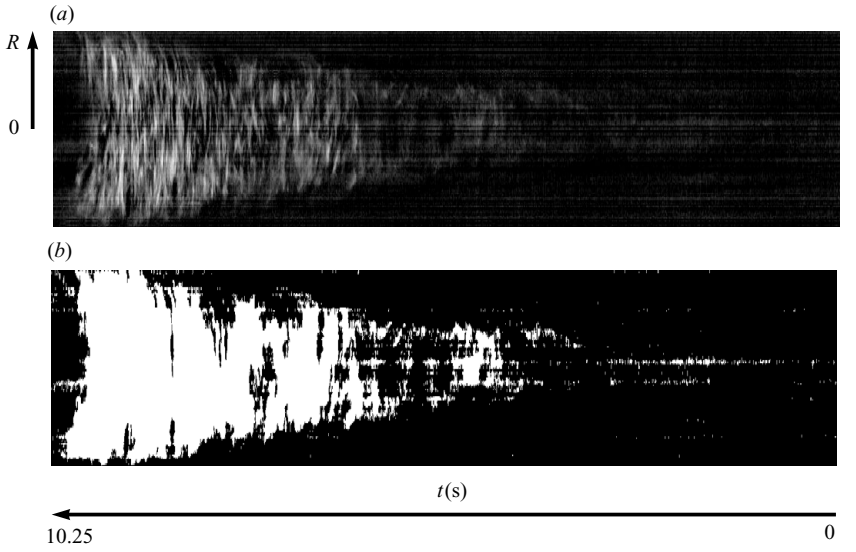

FIGURE 10. Space–time plot for 0.65 % glycerin at $Re_G = 2183$: (*a*) obtained from raw flow images and (*b*) obtained from filtered, background subtracted and binarized images. The puff length is ∼4.35 m. The image sequence consisted of 4100 frames.

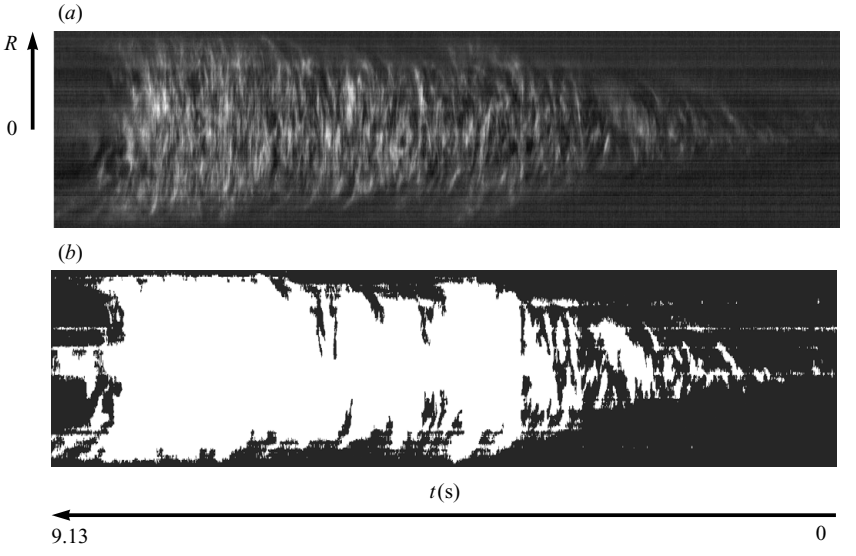

FIGURE 11. Space–time plot for 0.05 % Xanthan at $Re_G = 1984$: (*a*) obtained from raw flow images and (*b*) obtained from filtered, background subtracted and binarized images. The puff length is ∼2.5 m. The image sequence consisted of 3650 frames.

spatio-temporal plots of the images. Here the images are filtered and the variation of grey-scale intensity at one axial position is reported as a function of time (see figures 10–12). What is clear in this sequence of images is that an asymmetry is evident in the Carbopol example. The leading edge of the puff is elongated, in comparison to the Newtonian case, and is located near the wall.

Fluid	*Concentration* (wt%)	U_b ($m\,s^{-1}$)	u_c/U_b	Re_G	U_l/U_b	U_t/U_b	ℓ_{puff}/D
Glycerin	0.65	0.247	2	2143	1.73	0.76	86
Glycerin	0.65	0.252	2	2183	1.77	0.74	86
Glycerin	0.65	0.272	2	2357	1.73	0.74	88
Xanthan	0.05	0.165	1.98	1984	1.77	1.18	49
Xanthan	0.10	0.501	1.92	2236	1.73	1.17	52
Xanthan	0.20	1.185	1.72	1940	1.62	1.18	47
Carbopol	0.05 (pH 6.7)	0.927	1.78	2092	1.56	1.14	30
Carbopol	0.05 (pH 6.7)	0.968	1.78	2256	1.57	1.20	28
Carbopol	0.08 (pH 7.1)	1.514	1.73	1850	1.59	1.22	33
Carbopol	0.08 (pH 7.1)	1.576	1.73	2045	1.61	1.22	32
Carbopol	0.10 (pH 6.6)	2.184	1.69	2038	1.54	1.20	35
Carbopol	0.10 (pH 6.6)	2.266	1.69	2195	1.54	1.22	32

TABLE 4. Puff/slug characteristics for glycerin, Xanthan and Carbopol solutions. In this table we define U_l as the velocity of the leading edge and U_t as the velocity of the trailing edge.

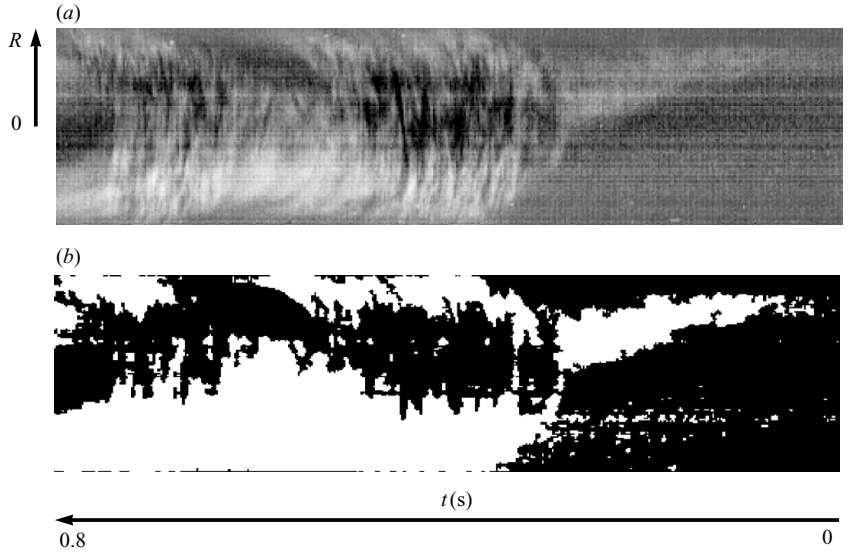

FIGURE 12. Space–time plot for 0.075 % Carbopol at $Re_G = 1850$: (*a*) obtained from raw flow images and (*b*) obtained from filtered, background subtracted and binarized images. The puff length is ~1.69 m. The image sequence consisted of 320 frames.

In table 4, we report typical sizes and velocities of puff from these images. For each fluid, around 2–4 puffs are analysed to produce table 4. With regards to the velocities we report separately the velocities of the leading and the trailing edges. These are measured in three different locations on the edges, namely at $r/R = 0$ and $r/R = \pm 0.75$. The fourth column in table 4 represents the centreline velocity in laminar regime just before the first puff is seen. What is evident from the data is that our estimates of the leading edge velocities for the non-Newtonian fluids are quite comparable to those measured for glycerin, as well as to those measured for Newtonian fluids by other investigators (see the summary in table 1). In contrast, the trailing edge velocities for the non-Newtonian fluid appear to be significantly faster than those for Newtonian

fluids. One possible interpretation of this is that the leading edge propagates by the same mechanism in all these fluids, i.e. controlled by spreading of turbulence structures within the puff, whereas the trailing edge is affected by relaminarisation, and hence the fluid rheology. Regardless of the correctness of this interpretation, the data suggest that puffs in the non-Newtonian fluids will spread axially at a significantly slower rate than those in Newtonian fluids. Another observation noted for the Carbopol solutions is that the elongation of the leading edge gets smaller with decreasing concentrations of Carbopol, i.e. the tip that we see in figure 12 is both reduced and gets closer to the centreline. It is also worth commenting that since the velocity profiles of shear-thinning fluids are flatter than Newtonian profiles, the difference between laminar and fully turbulent centreline velocities is reduced. Hence use of centreline velocity measurements to identify puff/slug occurrence does not give the same distinct 'signatures' as for Newtonian fluids. Therefore, rather than distinguishing between puff and slug, we simply use the term puff. Finally we comment that although we have made estimates of puff size, it is difficult to interpret these as it is highly dependent on the location of its origin and the time to the observation point – this is highly variable. We report these values here for completeness.

To summarize our observations, we measured the axial velocity as a function of radial position using LDV of three different classes of fluids undergoing Hagen–Poiseuille flow. We find that for the non-Newtonian fluids tested there is a persistent asymmetry in the velocity profiles present during transition. This asymmetry is also seen in r.m.s. profiles. Symmetrical flows were found for both laminar and fully turbulent cases. These observations were confirmed using high-speed imaging. No physical explanation is given at this point. We do, however, attempt to quantify transition more precisely by presenting a more in-depth statistical analysis of these results. We do so in the following subsection.

3.2. *Statistics of weak turbulence*

Landau & Lifschitz (1987) indicate that turbulent flows are traditionally characterized by random fluid motion in a broad range of temporal and spatial scales. In this section we attempt to characterize these scales using a number of different statistical measures given by Frisch (1995). By doing so we attempt to further characterize the differences in the behaviours of these three classes of fluids during transition.

To begin with, the first statistical measure we use is an autocorrelation function $C(\boldsymbol{\tau})$ defined by

$$C(\boldsymbol{\tau}) = \frac{< u(t)u(t+\boldsymbol{\tau}) >_{\boldsymbol{\tau}}}{u_{rms}^2} \tag{3.1}$$

and determined using the LDV data. This parameter is a measure of the time over which $u(t)$ is correlated with itself. In other words, $C(\boldsymbol{\tau})$ is bounded by unity as $\boldsymbol{\tau}$ approaches zero and by zero as $\boldsymbol{\tau} \to \infty$, because a process becomes uncorrelated with itself after a long time. We report the autocorrelation function as a function of Re_G and the radial position in the pipe. Representative results of this curve for the three fluids are given in figures 13–15. Before we proceed to interpret these figures we must spend some time explaining how the data is represented. Each figure is given as three panels, i.e. at three different radial positions. Within each panel four data sets are presented representing four different Reynolds numbers. The data series labelled (1) and (2) represent laminar flow while (3) is in transition and (4) in turbulence. With regards to (1), which is at the lowest Re_G, in each of the panels the velocity signal is probably dominated by high frequency noise which results in a fast decay of $C(\boldsymbol{\tau})$ with a characteristic decay time which we find to be of the order of the

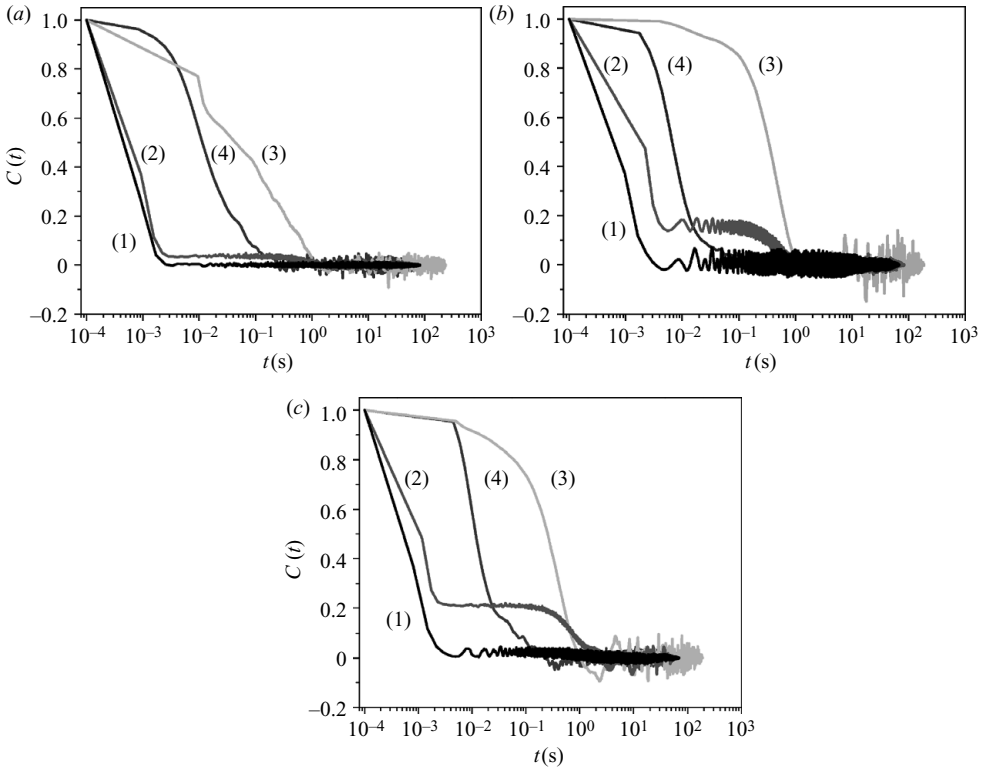

FIGURE 13. Correlation functions for a 80 % glycerin solution at three different radial positions (*a*) $r/R = -0.75$, (*b*) $r/R = 0$ and (*c*) $r/R = 0.75$. The data sets are: (i) $Re = 1174$, (ii) $Re = 1737$, (iii) $Re = 2201$ and (iv) $Re = 3546$.

inverse data rate of the signal. Proceeding through (4) we find the fully turbulent state characterized by rapid decay of the autocorrelation to the noise level.

A striking difference is found in curve (2) in comparison to the other curves. We observe that there are plateaus in these curves, for some radial positions for each of the fluids, e.g. at $C(\tau) \sim 0.4$ for both $r/R = \pm 0.75$ in the case of the Carbopol solution. Although this data was obtained in a region which we define as laminar, it is clear that there are some weakly correlated structures at this position in the pipe. For the Newtonian fluid, the plateau in the autocorrelation is at a lower value than that for the non-Newtonian fluids and is visible also at the centreline. For the non-Newtonian fluids the plateau is strongly attenuated at the centreline, but evident at the radial positions $r/R = \pm 0.75$. Using Taylor's frozen flow hypothesis (Taylor 1938) we may estimate the axial length scale of these structures to be $\sim 10^{-1}$ m, being longer for the Newtonian fluids than for the non-Newtonian fluids. This is significantly lower than the size of the puffs and slugs we report in table 4. We also comment that asymmetry is observed in many of the autocorrelation curves.

The second statistical measure we examined is the probability distribution of the velocity fluctuations. Again we report these results at three different radial positions for a number of Re_G (see figure 16). Like the autocorrelation, we present the data in three panels representing the different radial positions: at each radial position a number of different Re_G numbers are displayed. Each data set (roughly 10^5 velocity events were accounted for in the statistics) is normalized by the maximum count and

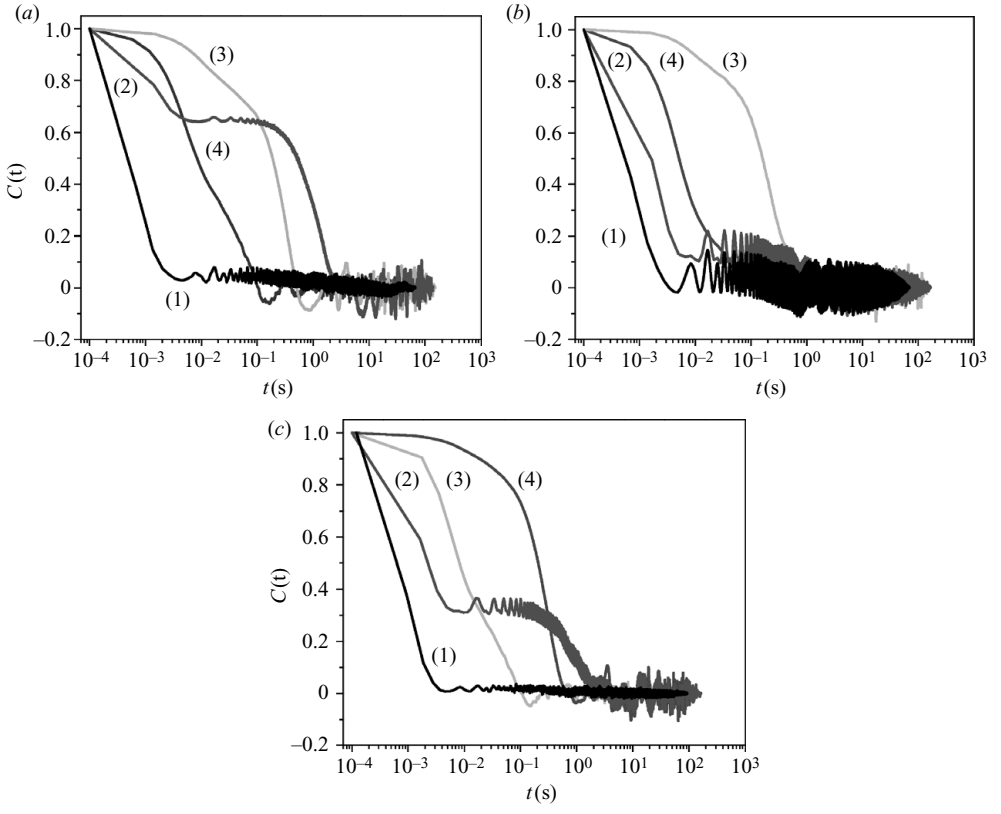

FIGURE 14. Correlation functions for a 0.2 % Xanthan solution at three different radial positions: (*a*) $r/R = -0.75$, (*b*) $r/R = 0$ and (*c*) $r/R = 0.75$. The data sets are: (i) $Re_G = 858$, (ii) $Re_G = 1218$, (iii) $Re_G = 2363$ and (iv) $Re_G = 5736$.

plotted against the reduced variable $[u(t) - \bar{U}]/u_{rms}$. Clearly, there is no statistical difference in these probability distributions when compared at different Re_G at similar radial positions, or at different radial positions and with similar Re_G. This finding holds for all classes of fluids tested.

Although intermittent flow behaviour is observed during our experiments in both pre-transitional and fully developed turbulent regimes, the physics underlying the two phenomena is substantially different. Whereas in the first case it is probably due to the emergence and dynamics of large-scale flow structures, the second case remains an open problem in fluid dynamics. In order to get a flavour of how non-Newtonian fluid rheology influences the emergence and magnitude of intermittency, we focus on higher order statistical flow properties for each of the three fluids under study, corresponding to the largest value of Re investigated.

At this point we turn our attention to the main findings in this section, an examination of the intermittency of transitional flow. An intriguing and partially understood feature of inertial turbulent flows is the emergence of intermittency which, simplistically speaking, manifests itself by 'rare' velocity bursts. In the case when a complex fluid is used, it is even less well understood how the non-Newtonian fluid rheology influences this phenomenon. Although the signature of this effect is somewhat visible in the tails of the probability distribution functions displayed in figure 16, a more systematic analysis requires the calculation of the velocity structure

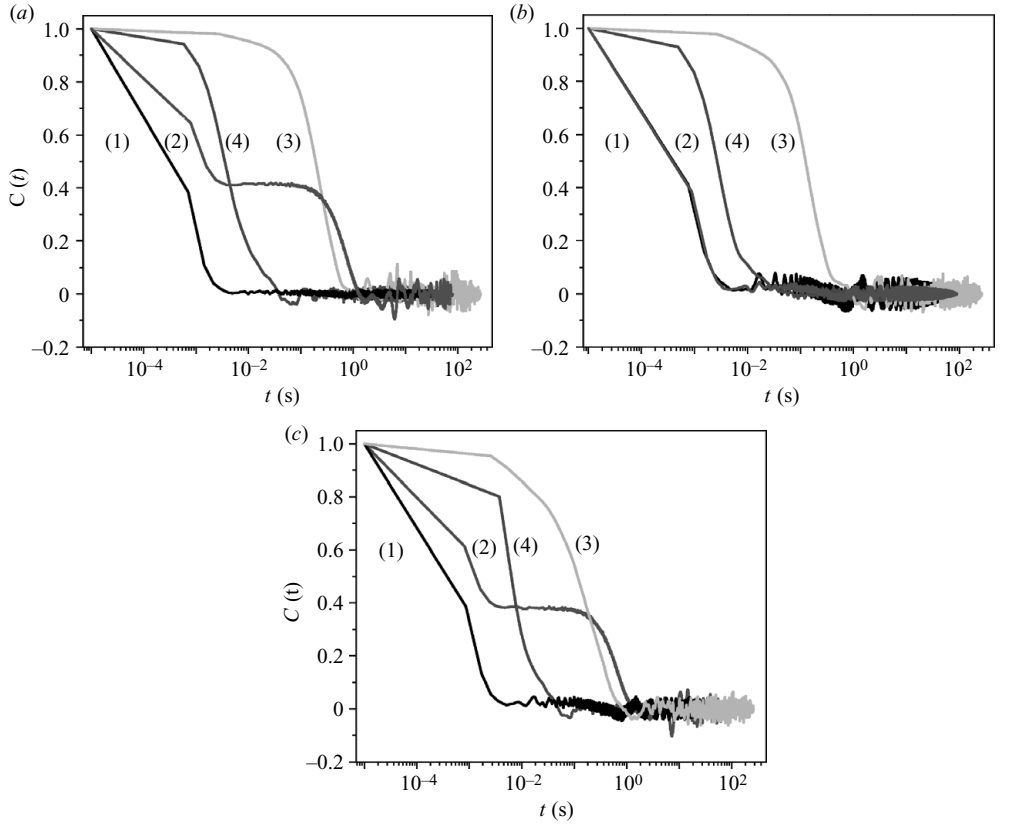

FIGURE 15. Correlation functions for a 0.1 % solution Carbopol at three different radial positions (*a*) $r/R = -0.75$, (*b*) $r/R = 0$ and (*c*) $r/R = 0.75$. The data sets are: (i) $Re_G = 397$, (ii) $Re_G = 914$, (iii) $Re_G = 2238$ and (iv) $Re_G = 3309$.

functions ξ_k, defined by

$$\xi_k(t) = \langle |u(\boldsymbol{\tau} + t) - u(\boldsymbol{\tau})|^k \rangle_{\boldsymbol{\tau}}, \tag{3.2}$$

as given by both Lesieur (1990) and Frisch (1995). In a fully developed and homogeneous turbulent flow, the Kolmogorov theory in which intermittency effects are not accounted for predicts

$$\frac{\xi_k}{\xi_3} = \frac{k}{3}. \tag{3.3}$$

Thus, the magnitude of the intermittent effects can be quantified by the deviations from the Kolmogorov scaling. In the Newtonian case and in a fully developed turbulent regime the intermittency is highest away from the centreline (see figure 17) whereas in the non-Newtonian case, the intermittency level is similar at each of the radial positions we have investigated. This finding suggests that in the transitional regime, the yield stress fluid behaves simply as a shear-thinning fluid and the effect of the plug at this point should therefore be considered as negligible. Care must be taken when interpreting this figure as we are not in fully turbulent flow. The Kolmogorov scaling is included in this figure for illustrative purposes. The message of this figure is that the structured fluids, according to this statistical measure, behave similarly in transition.

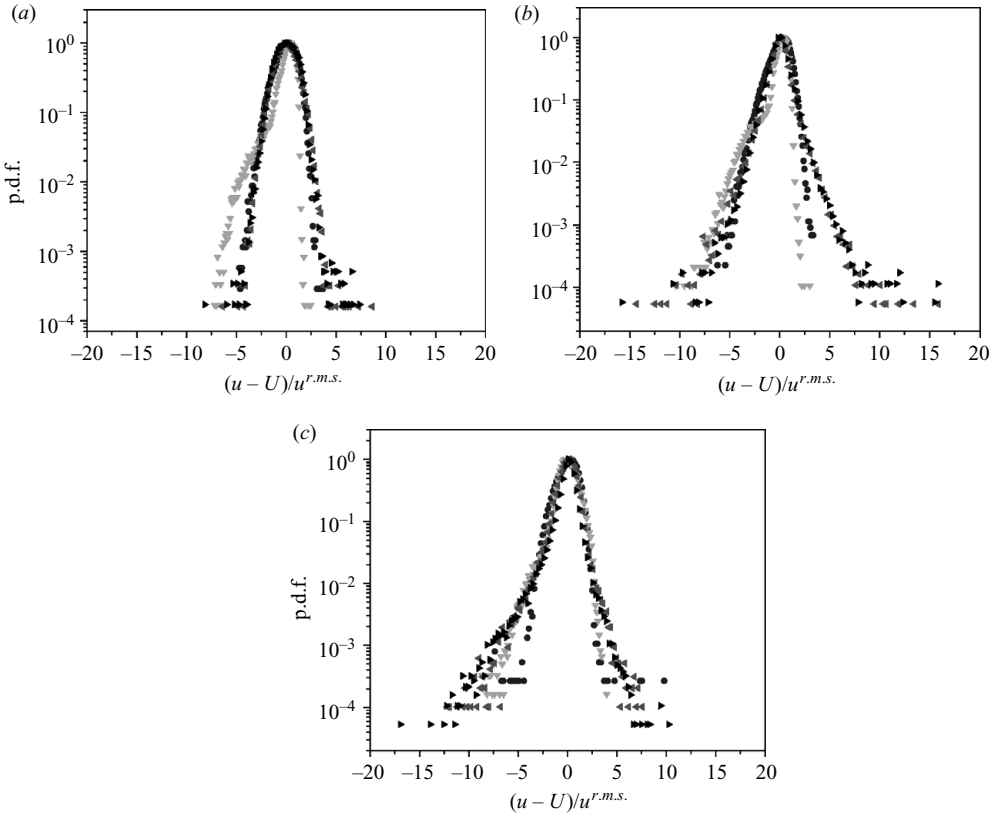

FIGURE 16. Velocity statistics for a 0.1 % Carbopol solution at three different radial positions (*a*) $r/R = -0.75$, (*b*) $r/R = 0$ and (*c*) $r/R = 0.75$. The symbols are: right triangles (►) $Re_G = 397$, left triangles (◄) $Re_G = 914$, up triangles (▼) $Re_G = 2238$, circles (●) $Re_G = 3309$.

This finding suggests that in the transitional regime, the yield stress fluid behaves simply as a shear-thinning fluid and the effect of the plug at this point should be considered negligible. This results from the fact that the size of the plug is below our detection limit.

4. The plug region during transition

For yield stress fluids the role of the plug region in retarding transition is largely unknown. If one interprets the yield stress fluid to be fully rigid below the yield stress then the laminar flow is analogous to that with the plug replaced by a solid cylinder moving at the appropriate speed. Presumably, since the effective viscosity becomes infinite at the yield surface the flow should be locally stabilized. Two different scenarios may be postulated at transition: (i) transition may occur in the yielded annulus around the plug, leaving intact the plug region; (ii) transition is retarded until the plug region thins to such an extent that the Reynolds stresses (in the annular region) can exceed the yield stress.

Scenario (i) is that described in Peixinho (2004) and Peixinho *et al.* (2005), where during the first stage of transition the turbulence intensity level on the centreline is reported as being similar to laminar levels. This is also the scenario assumed explicitly

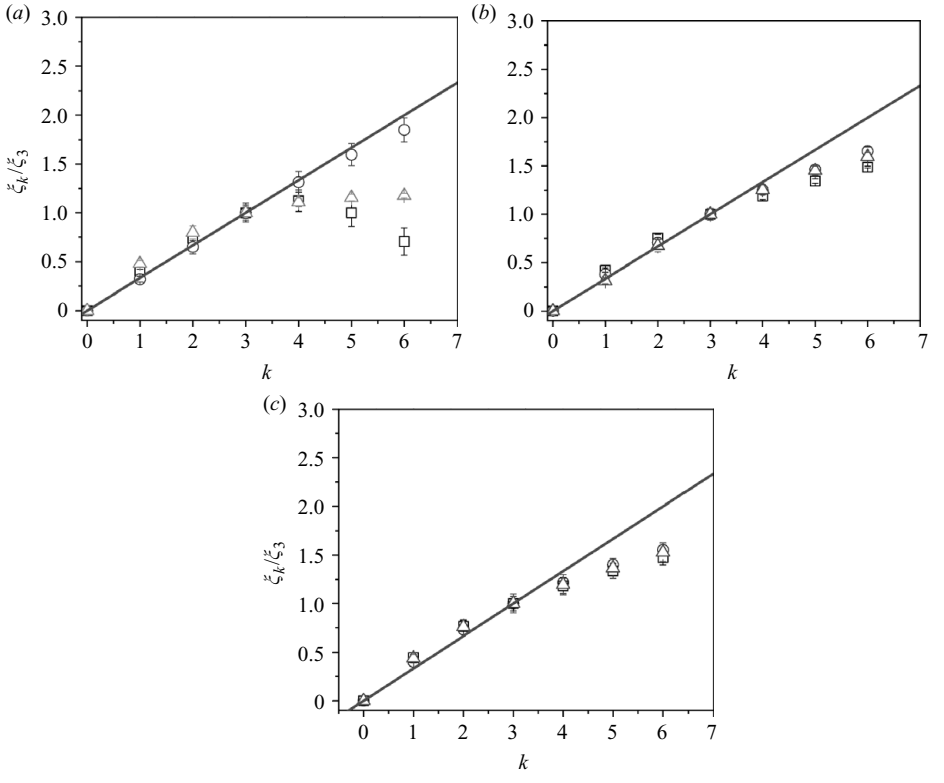

FIGURE 17. Deviations from the Kolmogorov scalings for (*a*) 80 % glycerin at $Re = 3456$, (*b*) 0.2 % Xanthan at $Re = 3513$ and (*c*) 0.1 % Carbopol at $Re = 2612$. The data is displayed at three different radial positions: □: $r/R = -0.75$, ○: $r/R = 0$ and △: $r/R = 0.75$.

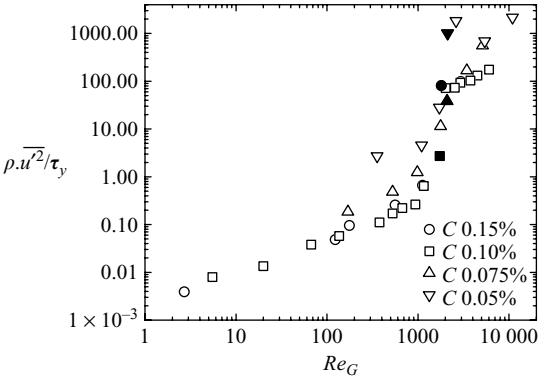

FIGURE 18. Axial Reynolds stresses normalized by yield stress for four different concentration levels of Carbopol. The filled symbols indicate points where the flow becomes transitional, with puffs/slugs first observed.

in some phenomenological theories of transition, e.g. Slatter (1999) treats the plug as a rigid body in developing his formula for transition.

In figure 18 we present the ratio of averaged Reynolds stress at the centreline (where the level of velocity fluctuations is minimum) to the yield stress, as a function of the

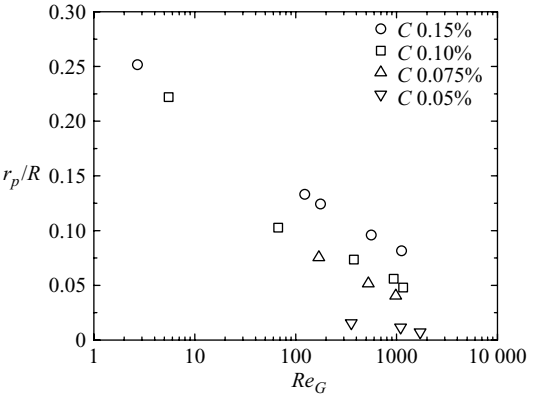

FIGURE 19. Plug radius normalized by pipe radius for four different concentration levels of Carbopol.

generalized Reynolds number Re_G for the four different Carbopol concentrations that we have used. The filled symbols in figure 18 mark the lowest value of Re_G for which puffs or slugs were detected in the experiments, for each of the different concentrations of Carbopol.

We can observe that the mean Reynolds stress exceeds the yield stress in each case. This remains true even if we subtract the laminar flow fluctuations from the Reynolds stresses, interpreting them as instrumental noise. This suggests to us that the second explanation given above is the more plausible, i.e. the plug has broken when transition starts. This is further reinforced by the results of the previous section on the structure functions, i.e. at these transitional/weak turbulent Reynolds numbers we have observed very similar intermittency characteristics with Carbopol, right across the pipe radius, as with Xanthan, where there is no yield stress. We should also comment that for the concentrations of Carbopol that we have used, if we calculate the (laminar) un-yielded plug diameters using

$$\frac{r_p}{R} = \frac{2L\tau_y}{R\Delta P}, \tag{4.1}$$

where L is the length of the pipe, for the largest flow rates for which puffs or slugs are not detected (see figure 19) these plug diameters are at most of the order 2 mm. Thus, we do not anyway have a *strong* plug close to transition.

There is no contradiction with the data from Peixinho (2004) and Peixinho *et al.* (2005), simply with its interpretation. Even with this thinning and breakup of the plug, in the Reynolds number range preceding transition flow instabilities are not sustained. Peixinho *et al.* (2005) report measuring low-frequency oscillations away from the central region. Such low-frequency forcing, presumably with slow axial variation could easily be responsible for slow extensional straining that yields the true plug of the base flow into a pseudo-plug. This type of psuedo-plug also occurs for example in thin film flows (Balmforth & Craster 1999), and in channels of slowly varying width (Frigaard & Ryan 2004). In such flows the velocity remains asymptotically close to the base flow solutions while shear and extensional stresses combine to maintain the pseudo-plug at just above the yield stress. Such flows are laminar but yielded and the psuedo-plug is characterized by large effective viscosity,

which would presumably give similar characteristics to the base laminar flow in controlling fluctuation level, as reported in Peixinho (2004) and Peixinho *et al.* (2005). From our measurements of the velocity profiles, the mean velocity remains very plug-like in the centre of the pipe in this upper range of laminar Reynolds numbers and it is simply not possible to discern whether what is observed is a true plug or not.

Evidently the ideal situation would be to visualize transition within a plug region of significant size in comparison to the pipe. Interestingly, this was the intention of our experiments. Our study was started after discussions with C. Nouar about ongoing experiments at LEMTA, Nancy, that were later reported in Peixinho (2004) and Peixinho *et al.* (2005). These were conducted in a 30 mm pipe at lower speeds, and for the flow rates at which transition occurred the plug region had radius of the order of 1 mm: too small to detect if broken or not. This prompted our interest in the role of the plug during transition, and we therefore designed our experiments at a larger scale so that we could potentially achieve transition with higher yield stress fluids, in larger diameter pipes and at higher speeds, hopefully also with a larger plug radius at transition. We were apparently defeated in this objective, as the small values of r_p/R in figure 19 indicate. Together with the experiments in Peixinho (2004) and Peixinho *et al.* (2005), our results contribute to the evidence that the plug region must thin to such an extent that the Reynolds stresses can break it, before transition commences.

5. Discussion and concluding remarks

In this work we measured the instantaneous velocity profiles of fully developed Hagen–Poiseuille flow using three different classes of fluids. The goal of this work was to develop a better understanding of transition in a yield stress fluid.

In § 3 of this work we characterized the flow field of the three different fluids and found that during transition, a persistent asymmetry was found both in the time-averaged velocity and in the local u_{rms} profiles. The asymmetry was confirmed by high-speed video imaging of the puffs and slugs from which we observed that the leading edge of the puff is elongated and located off the central axis of the pipe. Our findings are thus complementary to those reported in Escudier *et al.* (2005).

Initially we were sceptical about the physical mechanisms creating the asymmetry reported in Escudier *et al.* (2005), and about initial observations of the asymmetry in our own apparatus. We thus took all precautions possible to eliminate systematic bias. With regard to the Coriolis suggestions explored in Escudier *et al.* (2005), the Eckman numbers in our experiments were also large, Vancouver is at 49.26° North and the flow loop is oriented North–South. We found no evidence therefore to support this idea. In addition to the other potential factors discussed in Escudier *et al.* (2005), we also considered whether the optical properties of the fluids could affect the LDV measurements and whether extensional stresses transmitted backwards from the end tank (R_2) could be responsible. Eventually, our scepticism about these asymmetries has been rebuffed – we concur that they appear to be a fluid mechanical phenomenon. Perhaps the strongest evidence for this has come from the systematic and repeatable nature of the phenomena, but also with the asymmetries occurring for different fluids in different parts of the pipe.

In the context of our aim to study transitional phenomena in shear-thinning yield stress fluids, it is worth pointing out that the observed asymmetries have occurred with all structured fluids. While none of these is rheologically perfect as a generalized Newtonian fluid, the different fluids show different degrees of departure from this

ideal model, e.g. for laponite thixotropy is certainly the dominant feature, apart from the shear rheology, for Xanthan this would be visco-elasticity, etc. Thus, we suggest that it is the commonality of these fluids, i.e. the (largely inelastic) shear-thinning rheological behaviour, that is responsible for the asymmetry.

Recently, Esmael & Nouar (submitted) have offered an explanation for these asymmetries in terms of the existence of a robust nonlinear coherent structure characterized by two weakly modulated counter-rotating longitudinal vortices in the region (approximately) occupied by the sheared fluid. This explanation seems plausible in the light of recent developments in understanding of Newtonian fluid transition. To support this conclusion, Esmael & Nouar (submitted) have measured these structures both longitudinally and within the pipe cross-section, showing that there is a slow axial rotation of an otherwise modal structure with one-fold symmetry. The form of travelling wave solution is visually different to those computed for Newtonian fluids by Faisst & Eckhardt (2003) and Wedin & Kerswell (2004), but that should anyway be expected.

We concur with Peixinho (2004) and Peixinho *et al.* (2005) that transition takes place in a different manner than for Newtonian fluids, with a first stage in which the centreline velocity fluctuations are suppressed near to laminar levels while levels nearer the pipe wall increase significantly. The consequence of this is that if *r.m.s.* velocity or turbulence intensity components are to be monitored in order to detect transition, a radial position nearer the wall should be chosen, e.g. here $r/R = 0.75$, or $r/R = 0.8$ as advocated by Park *et al.* (1989) and Escudier *et al.* (1999).

We have reported our findings on characteristics of the puff/slugs, i.e. size and velocity of the leading and trailing edges. For yield stress fluids we have observed that the leading edges can be highly elongated and located off the central axis of the pipe. The other main finding here is that the trailing edges of puffs appear to move slower for the non-Newtonian fluids than for the Newtonian fluids reported in the literature. The leading edge velocities are similar to those for Newtonian fluids. The consequence of this is that puffs will spread slower in the axial direction as they travel along a pipe. We have not made a distinction in our work between puffs and slugs, referring simply to them all as puffs. This is because some distinguishing features in Newtonian fluids, e.g. the 'signature' changes in centreline velocity, are simply less clear for shear-thinning yield stress fluids. For such fluids the laminar and turbulent velocity profiles are closer to each other, meaning that abrupt changes in centreline velocity are reduced (see also Park *et al.* 1989; Peixinho *et al.* 2005).

We have also attempted to further characterize transition by examining both an autocorrelation function and a probability distribution function of the velocity fluctuations. The autocorrelation function shows some differences between the fluids, indicates weakly coherent unsteady structures located away from the axis in the non-Newtonian fluids and also indicates asymmetry. This occurs at Reynolds number that are high, but are still lower than we would normally expect for transition. For Newtonian fluids there is recent work on recurrent travelling waves at Reynolds numbers in these ranges, e.g. Kerswell & Tutty (2007). While our data may correspond to a non-Newtonian version of such structures, we have no strong evidence and prefer to leave the interpretation open to the reader. For the probability distribution functions there were no significant differences between the different classes of fluids examined.

Of more interest was the third statistical measure of the fluid we used, namely a structure function, in which we found that in transitional flow, the shear-thinning and yield stress fluids behaved somewhat similarly. This was the first indication that in

U (m s^{-1})	$\dot{\gamma}$ (s^{-1})	κ (Pa·s^n)	n	Re_G	T (°C)
0.2776	0.2–46	0.11	0.65	352	29
0.5396	0.5–90	0.11	0.65	858	29
0.7163	0.7–137	0.11	0.65	1218	29
0.9413	1–224	0.14	0.56	1900	29
1.1224	1–270	0.135	0.56	2363	30
1.4850	2–501	0.13	0.56	3244	30.5
2.2756	2–835	0.13	0.56	5736	31
3.4615	3–1311	0.13	0.56	10 197	34

TABLE 5. Flow conditions and power-law parameters for 0.2 % Xanthan gum.

U (m s^{-1})	$\dot{\gamma}$ (s^{-1})	κ (Pa·s^n)	n	Re_G	T (°C)
0.4613	0.1–82	0.23	0.56	451	30
0.6957	0.1–118	0.23	0.56	809	30
0.8775	1–192	0.22	0.56	1185	30
1.3574	2–598	0.20	0.56	2244	31
1.5616	1–635	0.14	0.64	2542	32
2.0574	1–692	0.11	0.69	3513	33
2.5877	1–988	0.10	0.69	5070	34

TABLE 6. Flow conditions and power-law parameters for 0.2 % Xanthan gum.

U (m s^{-1})	$\dot{\gamma}$ (s^{-1})	κ (Pa·s^n)	n	Re_G	T (°C)
0.3747	0.2–66	0.0235	0.77	1701	30
0.4529	0.3–78	0.0235	0.77	2131	31
0.4954	0.5–113	0.019	0.78	2789	32
0.5414	0.5–104	0.015	0.80	3538	33
0.8802	0.4–301	0.0103	0.80	8370	33
2.0203	2–757	0.0083	0.82	24 746	34

TABLE 7. Flow conditions and power-law parameters for 0.1 % Xanthan gum.

U (m s^{-1})	$\dot{\gamma}$ (s^{-1})	$\boldsymbol{\tau}_y$ (Pa)	κ (Pa·s^n)	n	r_p (mm)	Re_G	T (°C)
0.11202	0.1–24	2	2.05	0.36	5.55	5.5	29
0.4622	0.1–87	1.5	2.01	0.40	2.57	67	29
1.2076	1–220	1.4	1.59	0.43	1.84	378	29
2.0461	5–414	1.3	1.20	0.48	1.40	937	31
2.3218	5–472	1.2	0.92	0.53	1.20	1160	32.5
3.1146	5–657	1	0.65	0.60	—	1735	36
3.9005	5–1261	0.6	0.35	0.65	—	2920	39
4.3967	5–1559	0.4	0.20	0.70	—	4488	43

TABLE 8. Flow conditions and Herschel–Bulkley parameters for 0.1 % Carbopol.

transitional flow, the effect of the plug was minimal on the flow structure. In § 4 we have presented evidence that as transition occurs the plug actually thins to an extent where the Reynolds stresses are sufficient to break it.

The financial support of the Natural Sciences and Engineering Research Council of Canada (NSERC) is gratefully acknowledged as is that of the Canada Foundation for Innovation, New Opportunities Programme. We thank Chérif Nouar for numerous

U (m s^{-1})	$\dot{\gamma}$ (s^{-1})	τ_y (Pa)	κ (Pa·s^n)	n	r_p (mm)	Re_G	T (°C)
0.3093	0.2–62	1.80	1.11	0.50	4.11	42	34
1.0233	0.1–181	1.58	0.71	0.53	2.90	397	34
1.5457	0.1–267	0.95	0.60	0.54	1.67	914	34.5
2.3849	0.1–495	0.90	0.50	0.54	—	2001	36.5
2.5912	5–591	0.90	0.50	0.54	—	2238	37
3.0411	5–1063	0.52	0.39	0.58	—	2612	38
3.5002	3–1296	0.30	0.26	0.65	—	3309	39

TABLE 9. Flow conditions and Herschel–Bulkley parameters for 0.1 % Carbopol.

U (m s^{-1})	$\dot{\gamma}$ (s^{-1})	τ_y (Pa)	κ (Pa·s^n)	n	r_p (mm)	Re_G	T (°C)
0.1278	0.1–29	6.0	4.79	0.37	6.29	2.7	31
1.068	1–201	5.7	3.66	0.42	3.33	123	32
1.304	2–235	5.7	3.28	0.44	3.11	176	32
2.5573	0.4–480	5.6	2.87	0.46	2.40	561	35
3.6459	1–849	4.7	2.17	0.48	2.04	1120	39
3.7424	2–1065	1.7	1.7	0.48	—	1750	50
4.3054	2–1609	1.6	1.77	0.48	—	1804	45
4.8443	8–1816	0.72	0.93	0.52	—	2953	40

TABLE 10. Flow conditions and Herschel–Bulkley parameters for 0.15 % Carbopol.

U (m s^{-1})	$\dot{\gamma}$ (s^{-1})	τ_y (Pa)	κ (Pa·s^n)	n	r_p (mm)	Re_G	T (°C)
0.3902	0.6–70	0.38	0.37	0.58	1.89	170	30
0.7227	0.1–131	0.30	0.29	0.60	1.29	526	30
1.0754	3–195	0.28	0.26	0.61	1.01	984	30
1.4977	7–290	0.23	0.22	0.62	—	1770	31
1.697	2–358	0.21	0.21	0.63	—	2089	32
2.4452	0.1–864	0.12	0.16	0.65	—	3442	34
2.9218	6–1075	0.045	0.12	0.68	—	5134	36

TABLE 11. Flow conditions and Herschel–Bulkley parameters for 0.075 % Carbopol.

U (m s^{-1})	$\dot{\gamma}$ (s^{-1})	τ_y (Pa)	κ (Pa·s^n)	n	r_p (mm)	Re_G	T (°C)
0.1429	0.1–24	0.0065	0.0268	0.86	0.39	356	30
0.2792	1–49	0.0060	0.0188	0.86	0.29	1 098	30
0.4108	0.1–71	0.0052	0.0173	0.88	0.18	1 717	31
0.4736	3–103	0.0045	0.0153	0.90	—	2 114	30
0.5102	2–123	0.0040	0.0133	0.90	—	2 615	30
0.9108	0.7–393	0.0035	0.0110	0.91	—	5 409	30
1.4876	3–617	0.0025	0.0090	0.92	—	10 960	31

TABLE 12. Flow conditions and Herschel–Bulkley parameters for 0.05 % Carbopol.

fruitful discussions during visits both in Nancy & Vancouver during the course of this work.

Appendix. Fitted rheological parameters for the experiments conducted

We present below the fitted rheological parameters for the non-Newtonian fluids in our experiments. For each table we present the mean axial velocity U, the range

of shear rates over which data was measured in the rheometer in order to fit the parameters, the fitted rheological parameters, the radius of the plug (only if in laminar flow and with a yield stress fluid), the generalized Reynolds number and the temperature.

REFERENCES

Abbas, M. A. & Crowe, C. T. 1987 Experimental study of the flow properties of a homogeneous slurry near transitional Reynolds numbers. *Intl J. Multiphase Flow* **13** (3), 357–364.

Balmforth, N. J. & Craster, R. V. 1999 A consistent thin-layer theory for Bingham plastics. *J. Non-Newt. Fluid Mech.* **84**, 65–81.

Bandyopadhyay, P. R. 1986 Aspects of the equilibrium puff in transitional pipe flow. *J. Fluid Mech.* **163**, 439–458.

Berman, N. S. 1978 Drag reduction by polymers. *Annu. Rev. Fluid Mech.* **10**, 47–64.

Bewersdorff, H. W. 1991 Turbulence structure of dilute polymer and surfactant solutions in artificially roughened pipes. In *Sixth European Drag Reduction Working Meeting*, Eindhoven University of Technology.

Bird, R. B., Armstrong, R. C. & Hassager, O. 1987 *Dynamics of Polymeric Liquids, Volume 1: Fluid Mechanics*. Wiley.

Bogue, D. C. 1959 Entrance effects and prediction of turbulence in non-Newtonian flow. *Ind. Engng Chem.* **51**, 874–878.

Chapman, S. J. 2002 Subcritical transition in channel flows. *J. Fluid Mech.* **451**, 35–97.

Chen, R. Y. 1973 Flow in the entrance region at low Reynolds numbers. *J. Fluids Engng* **95**, 153–158.

Darbyshire, A. G. & Mullin, T. 1995 Transition to turbulence in contant-mass-flux pipe flow. *J. Fluid Mech.* **289**, 83–114.

Dodge, D. W. & Metzner, A. B. 1959 Turbulent flow of non-Newtonian systems. *A.I.Ch.E. J.* **5**, 189–204.

Doherty, J., Ngan, P., Monty, J. & Chong, M. 2007 The development of turbulent pipe flow. In *16th Australasian Fluid Mechanics Conference*, Gold Coast, Queensland, pp. 266–270.

Draad, A. A., Kuiken, G. D. C. & Nieuwstadt, F. T. M. 1998 Laminar-turbulent transition in pipe flow for Newtonian and non-Newtonian fluids. *J. Fluid Mech.* **377**, 267–312.

Draad, A. A. & Nieuwstadt, F. T. M. 1998 The Earth's rotation and laminar pipe flow. *J. Fluid Mech.* **361**, 297–308.

Draad, A. A. & Westerweel, J. 1996 Measurement of temporal and spatial evolution of transitional pipe flow with PIV. *Presentation at the meeting of the APS, Fluid Mechanics Section*, University of Buffalo, NY.

Durst, F., Ray, S., Unsal, B. & Bayoumi, O. A. 2005 The development lengths of laminar pipe and channel flows. *J. Fluids Engng* **127**, 1154–1160.

Eckhardt, B., Schneider, T., Hof, B. & Westerweel, J. 2007 Turbulence transition in pipe flow. *Annu. Rev. Fluid Mech.* **39**, 447–468.

Eliahou, S., Tumin, A. & Wygnanski, I. 1998 Laminar-turbulent transition in Poiseuille pipe flow subjected to periodic perturbation emanating from the wall. *J. Fluid Mech.* **361**, 333–349.

Escudier, M. P., Poole, R. J., Presti, F., Dales, C., Nouar, C., Desaubry, C., Graham, L. & Pullum, L. 2005 Observations of asymmetrical flow behaviour in transitional pipe flow of yield-stress and other shear-thinning liquids. *J. Non-Newt. Fluid Mech.* **127**, 143–155.

Escudier, M. P. & Presti, F. 1996 Pipe flow of a thixotropic liquid. *J. Non-Newt. Fluid Mech.* **62**, 291–306.

Escudier, M. P., Presti, F. & Smith, F. 1999 Drag reduction in the turbulent pipe flow of polymers. *J. Non-Newt. Fluid Mech.* **81**, 197–213.

Esmael, A. & Nouar, C. 2008 Transitional flow of a yield stress fluid in a pipe: evidence of a robust coherent structure. *Phys. Rev.* E **77**, 057302.

Faisst, H. & Eckhardt, B. 2003 Travelling waves in pipe flow. *Phys. Rev. Lett.* **91**, 224502.

Frigaard, I. A., Howison, S. D. & Sobey, I. J. 1994 On the stability of Poiseuille flow of a Bingham fluid. *J. Fluid Mech.* **263**, 133–150.

Frigaard, I. A. & Nouar, C. 2003 On three-dimensional linear stability of Poiseuille flow of Bingham fluids. *Phys. Fluids* **15**, 2843–2851.

Frigaard, I. A. & Ryan, D. P. 2004 Flow of a visco-plastic fluid in a channel of slowly varying width. *J. Non-Newt. Fluid Mech.* **123**, 67–83.

Frisch, U. 1995 *Turbulence: The legacy of A. N. Kolmogorov*. Cambridge University Press.

Froishteter, G. B. & Vinogradov, G. V. 1980 The laminar flow of plastic disperse systems in circular tubes. *Rheol. Acta.* **19**, 239–250.

Govier, G. W. & Aziz, K. 1972 *The Flow of Complex Mixtures in Pipes*. Van Nostrand-Reinhold.

Guo, B., Sun, K. & Ghalambor, A. 2004 A closed-form hydraulics equation for aerated-mud drilling in inclined wells. *SPE Dril. Compl.* **19** (2), 72–81.

Hamilton, J. M., Kim, J. & Waleffe, F. 1995 Regenaration mechanism of near-wall turbulence structures. *J. Fluid Mech.* **287**, 317–348.

Han, G., Tumin, A. & Wygnanski, I. 2000 Laminar-turbulent transition in Poiseuille pipe flow subjected to periodic perturbation emanating from the wall. Part 2. Late stage of transition. *J. Fluid Mech.* **419**, 1–27.

Hanks, R. W. & Pratt, D. R. 1967 On the flow of Bingham plastic slurries in pipes and between parallel plates. *SPE Paper No.* 1682.

Hof, B., vanDoorne, C. W. H., Westerweel, J. & Nieuwstadt, F. T. M. 2005 Turbulence regeneration in pipe flow at moderate Reynolds numbers. *Phys. Rev. Lett.* **95**, 214502.

Hof, B., vanDoorne, C. W. H., Westerweel, J., Nieuwstadt, F. T. M., Faisst, H., Eckhardt, B., Wedin, H., Kerswell, R. R. & Waleffe, F. 2004 Experimental observation of nonlinear traveling waves in turbulent pipe flow. *Science* **305**, 1594–1598.

Hof, B., Juel, A. & Mullin, T. 2003 Scaling of the turbulence transition threshold in a pipe. *Phys. Rev. Lett.* **91**, 244502-1-4.

Kerswell, R. R. & Tutty, O. R. 2007 Recurrence of travelling waves in transitional pipe flow. *J. Fluid Mech.* **584**, 69–102.

Landau, L. D. & Lifschitz, E. M. 1987 *Fluid Mechanics*. Pergamon Press.

Laufer, J. 1952 The structure of turbulence in fully developed pipe flow. *National Advisory Committee of Aeronautics, USA*, Report No. 1174.

Leite, R. J. 1959 An experimental investigation of the stability of Poiseuille flow. *J. Fluid Mech.* **5**, 81–96.

Lesieur, M. 1990 *Turbulence in Fluids Stochastic and Numerical Modelling* (*Fluid Mechanics and Its Applications*), 2nd rev. ed. Springer.

Mellibovsky, F. & Meseguer, A. 2007 Pipe flow transition threshold following localized impulsive perturbations. *Phys. Fluids* **19**, 044102.

Métivier, C., Nouar, C. & Brancher, J.-P. 2005 Linear stability involving the Bingham model when the yield stress approaches zero. *Phys. Fluids* **17**, 104106.

Metzner, A. B. & Reed, J. C. 1955 Flow of non-Newtonian fluids – correlation of the laminar, transition and turbulent-flow regions. *A.I.Ch.E. J.* **1**, 434–440.

Nguyen, Q. D. & Boger, D. V. 1985 Direct yield stress measurement with the vane method. *J. Rheol.* **29**, 335–347.

Nikuradse, J. 1932 Gesetzmassigkeiten der turbulenten stromung in glatten rohren, Forschung auf dem Gebiet des Ingenieurwesens. Translated in *NASA TT F-10, 359* (1966) **3**, 1–36.

Nouar, C. & Frigaard, I. A. 2001 Nonlinear stability of Poiseuille flow of a Bingham fluid. *J. Non-Newt. Fluid Mech.* **100**, 127–149.

Nouar, C., Kabouya, N., Dusek, J. & Mamou, M. 2007 Modal and non-modal linear stability of the plane Bingham—Poiseuille flow. *J. Fluid Mech.* **577**, 211–239.

Park, J. T., Mannheimer, R. J., Grimley, T. A. & Morrow, T. B. 1989 Pipe flow measurements of a transparent non-Newtonian slurry. *ASME J. Fluids Engng* **111** (3), 331–336.

Peixinho, J. 2004 Contribution expérimentale à l'étude de la convection thermique en régime laminaire, transitoire et turbulent pour un fluide à seuil en écoulement dans une conduite. PhD thesis, Université Henri Poincaré, Nancy, France.

Peixinho, J., Nouar, C., Desaubry, C. & Theron, B. 2005 Laminar transitional and turbulent flow of yield-stress fluid in a pipe. *J. Non-Newt. Fluid Mech.* **128**, 172–184.

Perry, A. E. & Abell, C. J. 1978 Scaling laws for pipe-flow turbulence. *J. Fluid Mech.* **67**, 257–271.

Poole, R. J. & Ridley, B. S. 2007 Development-length requirements for fully developed laminar pipe flow of inelastic non-newtonian liquids. *J. Fluids Engng* **129**, 1281–1287.

Reddy, S. C., Schmid, P. J. & Henningson, D. S. 1993 Pseudospectra of the Orr-Sommerfeld operator. *SIAM J. Appl. Maths* **53**, 15–47.

Reynolds, O. 1883 An experimental investigation of the circumstances which determine whether the motion of water shall be direct or sinuous, and the law of resistance in parallel channels. *Phil. Trans. R. Soc. Lond.* **174**, 935–982.

Rudman, M., Blackburn, H. M., Graham, L. J. W. & Pullum, L. 2004 Turbulent pipe flow of shear-thinning fluids. *J. Non-Newt. Fluid Mech.* **118**, 33–48.

Shah, S. N. & Sutton, D. L. 1990 New friction correlation for cements from pipe and rotational-viscometer data. *SPE Prod. Engng* **5** (4), 415–424

Shan, H., Ma, B., Zhang, Z. & Nieuwstadt, F. T. M. 1999 Direct numerical simulation of a puff and a slug in transitional cylindrical pipe flow. *J. Fluid Mech.* **387**, 39–60.

Slatter, P. T. 1999 The laminar-turbulent transition in large pipes. *International Conference Problems in Fluid Mechanics and Hydrology*, Prague, pp. 247–256.

Slatter, P. T. & Wasp, E. J. 2000 The laminar-turbulent transition in large pipes. *Proceedings of 10th International Conference on Transport and Sedimentation of Solid Particles*, Wroclaw, Poland, pp. 389–399.

Soto, R. J. & Shah, V. L. 1976 Entrance flow of a yield-power law fluid. *Appl. Sci. Res.* **32**, 73–85.

Taylor, G. I. 1938 The spectrum of turbulence. *Proc. R. Soc. London, Ser.* A **164**, 476.

Teitgen, R. 1980 Laminar-turbulent transition in pipe flow: development and structure of the turbulent slug. *Laminar-Turbulent Transition, IUTAM Symposium*, Stuttgart, Germany, vol. 1979, pp. 27–36. Springer.

Toonder, J. M. J. & Nieuwstadt, F. T. M. 1997 Reynolds number effects in a turbulent pipe flow for low to moderate *Rev. Phys. Fluids* **9**, 3398–3409.

Trefethen, L. N., Trefethen, A. E., Reddy, A. E. & Driscoll, T. A. 1993 Hydrodynamic stability without eigenvalues. *Science* **261**, 578–584.

Turian, R. M., Ma, T. W., Hsu, F. L. G. & Sung, D. J. 1998 Experimental study of the flow properties of a homogeneous slurry near transitional Reynolds numbers. *Intl J. Multiphase Flow* **13** (3), 357–364.

Waleffe, F. 1997 On a self-sustaining mechanism in shear flows. *Phys. Fluids* **9**, 883–900.

Wedin, H. & Kerswell, R. R. 2004 Exact coherent solutions in pipe flow : travelling wave solutions. *J. Fluid Mech.* **508**, 333–371.

White, C. M. & Mungal, M. G. 2008 Mechanics and prediction of turbulent drag reduction with polymer additives. *Annu. Rev. Fluid Mech.* **40**, 235–256.

White, F. M. 1999 *Fluid Mechanics*, 4th ed. McGraw-Hill.

Willingham, J. D. & Shah, S. N. 2000 Friction pressures of Newtonian and non-Newtonian fluids in straight and reeled coiled tubing. *SPE Paper No.* 60719-MS. *Proceedings of the SPE/ICoTA Coiled Tubing Roundtable*, 5–6 April 2000, Houston, TX.

Wilson, K. C. & Thomas, A. D. 1985 A new analysis of the turbulent flow of non-Newtonian fluids. *Can. J. Chem. Engng* **63**, 539–546.

Wilson, K.C. & Thomas, A. D. 2006 Analytic model of laminar-turbulent transition for Bingham plastics. *Can. J. Chem. Engng* **84** (5), 520–526.

Wygnanski, I. J. & Champagne, F. H. 1973 On transition in a pipe. Part 1. The origin of puffs and slugs and the flow in a turbulent slug. *J. Fluid Mech.* **59**, 281–335.

Wygnanski, I. J., Sokolov, M. & Friedman, D. 1975 On transition in a pipe. Part 2. The equilibrium puff. *J. Fluid Mech.* **69**, 283–304.